International Forum on Aeroelasticity and Structural Dynamics
IFASD 2017
25-28 June 2017 Como, Italy

RESPONSE AND STABILITY OF THE REMOTELY-PILOTED, CONSTRAINED X-HALE AIRCRAFT IN WIND TUNNEL

Antônio B. Guimarães Neto[1], Flávio J. Silvestre[1], Flávio L. S. Bussamra[1], Roberto G. A. da Silva[1], Carlos E. S. Cesnik[2]

[1]Instituto Tecnológico de Aeronáutica
São José dos Campos, SP, 12228-900, Brazil
antoniobgn@gmail.com
flaviojs@ita.br
flaviobu@ita.br
gil@ita.br

[2]Department of Aerospace Engineering
University of Michigan, Ann Arbor, Michigan, 48109-2140
cesnik@umich.edu

Keywords: aeroelasticity, flight dynamics, flexible aircraft, wind tunnel

Abstract: Formulations for the flight dynamics of flexible aircraft have been commonly applied to aircraft free to fly in the three-dimensional space, having all six rigid-body degrees of freedom. For risk reduction in the future flight operations of the X-HALE testbed at ITA, however, wind-tunnel tests of the remotely-piloted, four-meter-span configuration of the aircraft were performed. In the wind tunnel, the rigid-body translations were completely constrained, but the same was not valid for the rigid-body rotations, which could be conveniently left free or not with a proper selection of the connection between the aircraft and the wind-tunnel mount. In the present paper, in order to computationally assess the response and stability characteristics of the aircraft in the wind tunnel, we derive equations of motion for a constrained flexible aircraft with up to three rigid-body rotational degrees of freedom, mounted on an also flexible wind-tunnel strut. The numerical model has its value confirmed by the wind-tunnel tests in the predicted and observed roll-control reversal for anti-symmetrical deflections of the all-moving tails, and absence of reversal for aileron deflections.

1 INTRODUCTION

The inclusion of elastic degrees of freedom in the formulation of the flight dynamics of aircraft becomes more necessary as the aircraft structures present improved structural strength but reduced weight and stiffness. In flexible aircraft, the dynamic coupling between the rigid-body motion and the elastic deformation occurs more easily, and neglecting it may result in unacceptable error levels in simulation models.

A comprehensive literature review of the different formulations available for the flight dynamics of flexible aircraft was provided by Guimarães Neto et al. [1]. The dynamically-coupled formulations were classified as those in which n elastic degrees of freedom (DOFs) are included in the mathematical model of the aircraft, representing its structural dynamics; consequently, the number of equations of motion (EOMs) increases as the classical six-degree-of-freedom (6-DOF) rigid-body system is converted to an arbitrary (6+n)-DOF system.

Bisplinghoff, Ashley and Halfman [2], Bisplinghoff and Ashley [3], and Etkin [4] were among the first to derive dynamically-coupled but inertially-decoupled formulations [1]. However, formulations of this kind would only be used in practical applications more than a decade later due to the necessary development of electronic computing resources. The FLEXSTAB [5, 6] system of computer programs developed at the Boeing Company from the late 1960s to the middle 1970s deserves special mention, as it enabled an adequate prediction of the stability characteristics of elastic aircraft at both subsonic and supersonic speeds.

The introduction of n additional structural-dynamic degrees of freedom while keeping the classical six DOFs of the rigid body implies that constraints must be included in the formulations to eliminate the rigid-body DOFs from those of the structural-dynamic model. Such constraints are usually expressed by the choice of body axes. Milne [7] introduced more formalism to this important topic. In his report, three particular choices of body axes were discussed: attached, mean and principal axes.

The origin of the attached axes remains invested in one material point and the axes' directions may be tangent, normal and binormal to a curve of material points that contains the original point [7]. The mean axes were probably first defined by Lamb [8] in 1929: with respect to them, the linear and angular momenta of the elastic motion are identically zero at every instant. At last, the principal axes are those with respect to which the inertia matrix is diagonal at any instant [7].

Recently, the work of Guimarães Neto et al. [1] extended Milne's concept of attached axes to a more general form named dually-constrained axes, in which the origin of the structural axes (the point where elastic deformations are assumed null) does not necessarily coincide with the origin of the flight-dynamic body axes (with respect to which the EOMs are written). Attached axes became, then, a particular case when such coincidence occurs.

Rodden and Love [9] derived EOMs for a quasi-steady vehicle using the flexibility matrix of the restrained vehicle but calculating the orientation of the mean axes as a function of the deformation of the restrained structure. Their paper exerted a significant impact on computational aeroelasticity worldwide, since the solution sequence of MSC.Nastran for static aeroelasticity is based on their work [10]. More recently, Dykman and Rodden [11] derived EOMs considering dynamic aeroelastic effects as well, based on the modal superposition technique, and showed that a quasi-steady vehicle formulation can be obtained by the residualization of all modes of vibration.

Considering large rigid-body motions but small elastic deformations, Waszak and Schmidt [12] used Lagrange's equation to derive the same EOMs previously obtained in Refs. [3,4]. None of these are readily applicable to constrained vehicles.

It is highly desirable from a computational viewpoint that flight-dynamic formulations consider the finite-element method (FEM) in modeling the structural-dynamic EOMs. References [9] and [11] e.g. can be applied to FEM-modeled aircraft, but do not consider large rigid-body rotations. Cavin III and Dusto [13] developed FEM approximations with respect to a body mean-axis system in which collinearity between deformations and deformation velocities was assumed, but with small body angular rates.

Buttrill, Zeiler and Arbuckle [14] derived EOMs considering the availability of a lumped-mass FEM model and retained all the inertial coupling terms. Zeiler and Buttrill [15] refined the

EOMs using nonlinear strain-displacement relations to improve the calculation of the incremental stiffness matrix due to nonzero body angular rates – the centrifugal stiffening effect. However, in both studies [14, 15], the rotational DOFs of the lumped mass elements were not considered.

Meirovitch and Tuzcu [16] developed a modular dynamic formulation using Lagrange's equations for quasi-coordinates [17] to derive inertially-coupled, hybrid EOMs. The EOMs were then discretized in space for the solution of the boundary-value problem for the elastic deformation. The formulation, however, is not easily adaptable to the employment of lumped-mass FEM models with rotational DOFs [18, 19].

Reschke [19, 20] also used Lagrange's equations for quasi-coordinates in the derivation of EOMs, and had in mind the direct integration with FEM models. Differently from Refs. [14,15], the author considered the rotational DOFs of the FEM nodes. All inertial coupling terms were derived. The elastic DOFs were represented by free-free modes of vibration, making some but not all of the inertial coupling terms vanish, and variations of the inertia matrix were allowed.

Baldelli, Chen and Panza [21] used rational function approximations (RFAs) to develop a unified aeroelastic and flight-dynamic formulation aimed at control system design. Higher-fidelity quasi-steady aerodynamic data and gravity terms were used to modify the RFAs. The use of unsteady aerodynamics generates a full-frequency flight dynamic model, in which the rigid-body modes are subject to high-frequency unsteady aerodynamic effects usually not considered in flight dynamics. However, the EOMs are essentially linear due to the linear transformations used from the body axes to the stability axes and also due to the linear character of the RFAs nonlinear effects in the quasi-steady aerodynamic coefficients are not present. These issues would be of concern in flight simulation applications.

Guimarães Neto [22] derived equations of motion neglecting none of the inertial-coupling terms, and which can be readily applied to aircraft with lumped-mass FEM models. The inertial-coupling terms were however linearized with respect to the structural degrees of freedom, inspired by the method of Hesse and Palacios [23]. Consistent RFAs [24] were used to represent the unsteady aerodynamic effects calculated with the doublet-lattice method [25].

Wind-tunnel testing of clamped aeroelastic models has been common practice for decades, and for such models only the aeroelastic equations of motion do actually matter. On the other hand, devices such as the classical Pitch and Plunge Apparatus (PAPA) [26] used in NASA's Transonic Dynamics Tunnel (TDT) were developed to conduct two-degree-of-freedom flutter research using rigid wings, and then do not correlate much with the proposition of the present paper.

To the best of the authors' knowledge, no previous work exists on the physical-mathematical modeling or on the experimental aspects of the wind-tunnel testing of a remotely-piloted aeroelastic aircraft. It is a fact that, for small rigid-body rotations, the formulations of Rodden and Love [9], Dykman and Rodden [11] or Baldelli, Chen and Panza [21], for example, can be applied in the assessment of the response of vehicles with motion constrained in a wind tunnel. However, arbitrarily-large angular excursions result in nonlinearities in the rigid-body rotational kinematics that would not be considered in such formulations, as well as nonlinearities in the aerodynamic forces and moments would be more difficultly included. Moreover, a theoretical advantage exists in the derivation of the equations of motion from first principles, avoiding the need to perform adaptations that can be cumbersome.

The equations of motion are derived using Lagrange's equations with holonomic constraints [17, 28]. Structural flexibility of both the aircraft and the wind-tunnel mount is allowed, represented by a finite-element model with lumped-mass elements and beam elements for small deformations. In principle, all aircraft rigid-body degrees of freedom are included, but the corresponding constraint equations need also be considered. The rotational degrees of freedom are modeled as the Euler angles of the body reference frame (BRF).

The developed formulation is applied to the four-meter-span X-HALE configuration [27], with the objective of determining the general response and stability characteristics of the aircraft in the IAE (Instituto de Aeronáutica e Espaço, Portuguese for Institute of Aeronautics and Space) TA-2 subsonic wind tunnel in São José dos Campos, Brazil. Correlation with experimental data is presented.

2 DERIVATION OF THE EQUATIONS OF MOTION

In the equations of motion to be derived in this section, the aircraft is, in the most general case, assumed to be connected with $6 - n_c$ free degrees of freedom to the extremity of a flexible mount (strut), which is itself clamped in its other extremity to the wind-tunnel wall. Therefore, the whole aeroelastic system consisting of the aircraft plus the flexible mount is subjected to $12 + n_c$ constraints. Six constraints refer to the clamp of the flexible mount to the wind-tunnel wall; other six refer to equations that define the aircraft body axis system with respect to the structural motion; and n_c refer to the aircraft-mount connection constrained degrees of freedom.

The body reference frame (BRF) is related to the aircraft only, with a corresponding coordinate system given by a set of orthonormal basis vectors that form the columns of a matrix $\mathfrak{F}_b$. This set of axes is known as the body axes. Because the basis vectors are orthonormal, $\mathfrak{F}_b$ is an orthogonal matrix: ${\mathfrak{F}_b}^{-1} = {\mathfrak{F}_b}^T$.

The mount reference frame (MRF) is considered to coincide with the inertial reference frame (IRF) of the assumed flat and non-rotating Earth [29], an excellent approximation for the aircraft dynamics in the wind tunnel. With no loss of generality, the IRF orthonormal basis vectors are assumed to be unit vectors in each of the three dimensions, the columns of a matrix $\mathfrak{F}_0 = \mathbf{I}_3$. This set of axes is known as the inertial axes, the origin of which is considered to be at $\mathbf{0}_{3\times1}$. A generic vector $\mathbf{v}$ can be written in such a frame as:

$$\mathbf{v} = \mathfrak{F}_0 \mathbf{v}_0 = \mathbf{I}_3 \mathbf{v}_0. \tag{1}$$

The same generic vector $\mathbf{v}$ can also be written as $\mathfrak{F}_b \mathbf{v}_b$, from which the following transformation of coordinates is obtained:

$$\mathbf{v}_b = {\mathfrak{F}_b}^T \mathfrak{F}_0 \mathbf{v}_0 = \mathbf{C}_{b0} \mathbf{v}_0. \tag{2}$$

The transformation matrix $\mathbf{C}_{b0}$ from the inertial frame to the body frame is obtained by a classical sequence (3-2-1) of Euler rotations, ψ, θ and ϕ [29], and is given by:

$$\mathbf{C}_{b0} = \begin{bmatrix} \cos\theta\cos\psi & \cos\theta\sin\psi & -\sin\theta \\ \cos\psi\sin\theta\sin\phi - \sin\psi\cos\phi & \sin\psi\sin\theta\sin\phi + \cos\psi\cos\phi & \cos\theta\sin\phi \\ \cos\psi\sin\theta\cos\phi + \sin\psi\sin\phi & \sin\psi\sin\theta\cos\phi - \cos\psi\sin\phi & \cos\theta\cos\phi \end{bmatrix}. \tag{3}$$

The equations of motion for the flexible system with $12 + n_c$ constrained degrees of freedom can be derived using Lagrange's equations with holonomic constraints [28]:

$$\frac{d}{dt}\left(\frac{\partial \mathcal{L}}{\partial \dot{q}_i}\right) - \frac{\partial \mathcal{L}}{\partial q_i} + \frac{\partial \mathcal{F}}{\partial \dot{q}_i} = \sum_{k=1}^{12+n_c} \lambda_k \frac{\partial f_k}{\partial q_i} + Q_i, \tag{4}$$

where $\mathcal{L} = T - U$ is the Lagrangian; $\mathcal{F}$ is Rayleigh's dissipation function; f_k, $k = 1, 2, \cdots, 12+n_c$, are the functions describing the constraints of the system; λ_k are the corresponding Lagrange multipliers; q_i, $i = 1, 2, \cdots, 6 + n$, are the $6 + n$ generalized coordinates of the system; and Q_i are the corresponding nonpotential generalized forces.

The generalized coordinates q_i constitute a vector $\mathbf{q}$. By definition, the holonomic constraints depend only on the generalized coordinates and time:

$$f_k = f_k\left(\mathbf{q}, t\right), (k = 1, 2, \cdots, 12 + n_c). \tag{5}$$

The elected set of $6 + n$ generalized coordinates for the flight dynamics of the flexible system comprises: the components of the position vector $\mathbf{R}_{O,b}$ of the origin O of the BRF, expressed in the body axes, b: $\mathbf{R}_{O,b} = \begin{Bmatrix} x_O & y_O & z_O \end{Bmatrix}^T$; the Euler angles providing the orientation of the BRF with respect to the inertial reference frame (IRF): ψ, θ, and ϕ; and n elastic degrees of freedom of the whole system, constituting the displacement vector $\mathbf{u}_G = \begin{Bmatrix} u_1 & u_2 & \cdots & u_n \end{Bmatrix}^T$.

As in Ref. [1], the aeroelastic system is considered to be structural-dynamically represented by a finite-element model with lumped properties of inertia. The energy terms are calculated with integral expressions over the mathematical spatial domain V representing the whole system, but a convenient subdivision into the V_A sub-domain representing the aircraft, where body axes are used, and the V_M representing the flexible mount, where the inertial axes are used, is here appropriate. The integral expressions are given exactly by the sum of $N_m = N_{m,acft} + N_{m,mount}$ integrals over a collection of mutually-exclusive N_m sub-domains V_j. A sub-domain V_j contains one, and only one, mass element, and there exists no sub-domain without a mass element. Therefore, the total number of mass elements is also N_m. The CM of the jth mass element is at a point J. Besides J, the sub-domain V_j also contains an infinite quantity of generic points, each denoted by I.

The sub-domains V_j are considered to have no elastic deformation, with their internal rigid-body motion hence due solely to the elastic motion of a corresponding structural node K with which the CM of the mass element coincides ($K \equiv J$) or to which the mass element is rigidly attached.

The position vector of any point I in the aeroelastic system with respect to the origin of the IRF is then expressed by:

$$\mathbf{R}_I = \mathbf{R}_O + \mathbf{s}_{OK} + \mathbf{s}_{KJ} + \mathbf{s}_{JI} + \mathbf{d}_{OK} + \mathbf{d}_{KJ} + \mathbf{d}_{JI}, \tag{6}$$

where $\mathbf{s}_{(\bullet)}$ refers to the relative position vectors in the undeformed (unstrained) condition, usually called the jig shape; and $\mathbf{d}_{(\bullet)}$ stands for the changes in the $\mathbf{s}_{(\bullet)}$ vectors due to the structural deformation.

For points in the aircraft, the position vectors in Eq. (6) can then be written as:

$$\mathbf{R}_I|_{acft} = \mathfrak{F}_b \mathbf{R}_{I,b} = \mathfrak{F}_b \left(\mathbf{R}_{O,b} + \mathbf{s}_{OK,b} + \mathbf{s}_{KJ,b} + \mathbf{s}_{JI,b} + \mathbf{d}_{OK,b} + \mathbf{d}_{KJ,b} + \mathbf{d}_{JI,b} \right). \tag{7}$$

For points in the flexible mount, the position vectors in Eq. (6) are written as:

$$\mathbf{R}_I|_{mount} = \mathfrak{F}_0 \mathbf{R}_{I,0} = \mathfrak{F}_0 \left(\mathbf{s}_{OK,0} + \mathbf{s}_{KJ,0} + \mathbf{s}_{JI,0} + \mathbf{d}_{OK,0} + \mathbf{d}_{KJ,0} + \mathbf{d}_{JI,0} \right). \tag{8}$$

To calculate the kinetic energy, the velocity vectors are expressed in terms of time derivatives taken in the IRF:

$$\begin{aligned} {}^0\dot{\mathbf{R}}_I\Big|_{acft} = {}^0\dot{\mathfrak{F}}_b \left(\mathbf{R}_{O,b} + \mathbf{s}_{OK,b} + \mathbf{s}_{KJ,b} + \mathbf{s}_{JI,b} + \mathbf{d}_{OK,b} + \mathbf{d}_{KJ,b} + \mathbf{d}_{JI,b} \right) + \\ \mathfrak{F}_b \left({}^b\dot{\mathbf{R}}_{O,b} + {}^b\dot{\mathbf{d}}_{OK,b} + {}^b\dot{\mathbf{d}}_{KJ,b} + {}^b\dot{\mathbf{d}}_{JI,b} \right), \end{aligned} \tag{9}$$

$${}^0\dot{\mathbf{R}}_I\Big|_{mount} = \mathfrak{F}_0 \left({}^0\dot{\mathbf{d}}_{OK,0} + {}^0\dot{\mathbf{d}}_{KJ,0} + {}^0\dot{\mathbf{d}}_{JI,0} \right). \tag{10}$$

The following equations were derived in Ref. [1] and are used in the present development:

$${}^0\dot{\mathfrak{F}}_b = \mathfrak{F}_b \widetilde{\boldsymbol{\omega}_b}, \tag{11}$$

$$\widetilde{\boldsymbol{\omega}_b} = \mathbf{C}_{b0} \dot{\mathbf{C}}_{b0}^T, \tag{12}$$

with the skew-symmetric operator, $\widetilde{(\bullet)}$ or $\text{skew}\,(\bullet)$, providing an $\mathbb{R}^{3\times3}$ representation of a vector $(\bullet) \in \mathbb{R}^3$, in which, if $\mathbf{v} = \begin{Bmatrix} v_x & v_y & v_z \end{Bmatrix}^T \in \mathbb{R}^3$, then:

$$\widetilde{\mathbf{v}} = \text{skew}\,(\mathbf{v}) = \begin{bmatrix} 0 & -v_z & v_y \\ v_z & 0 & -v_x \\ -v_y & v_x & 0 \end{bmatrix}. \tag{13}$$

The vector $\boldsymbol{\omega}_b = \begin{Bmatrix} p & q & r \end{Bmatrix}^T$ is the angular velocity vector of the BRF with respect to the IRF, and has the components (body angular rates) p, q and r in the body axes. From Eqs. (3) and (12), one can express such components in terms of the vector of time derivatives of the Euler angles, $\dot{\boldsymbol{\varphi}} = \begin{Bmatrix} \dot{\phi} & \dot{\theta} & \dot{\psi} \end{Bmatrix}^T$:

$$\boldsymbol{\omega}_b = \begin{bmatrix} 1 & 0 & -\sin\theta \\ 0 & \cos\phi & \sin\phi\cos\theta \\ 0 & -\sin\phi & \cos\phi\cos\theta \end{bmatrix} \dot{\boldsymbol{\varphi}} = \mathbf{H}_{\varphi}{}^{-1} \dot{\boldsymbol{\varphi}} \tag{14}$$

From Eqs. (9), (11) and (12), the velocity vector of aircraft material points in the inertial frame becomes:

$$ {}^{0}\dot{\mathbf{R}}_I\Big|_{acft} = \mathfrak{F}_b \left({}^{b}\dot{\mathbf{R}}_{O,b} + \widetilde{\boldsymbol{\omega}_b}\mathbf{R}_{O,b} + {}^{b}\dot{\mathbf{d}}_{OI,b} + \widetilde{\boldsymbol{\omega}_b}\mathbf{s}_{OI,b} + \widetilde{\boldsymbol{\omega}_b}\mathbf{d}_{OI,b} \right), \tag{15} $$

where $\mathbf{s}_{OI,b} = \mathbf{s}_{OK,b} + \mathbf{s}_{KJ,b} + \mathbf{s}_{JI,b}$ and $\mathbf{d}_{OI,b} = \mathbf{d}_{OK,b} + \mathbf{d}_{KJ,b} + \mathbf{d}_{JI,b}$.

The elastic displacements of a node K are given by the translation vector $\mathbf{d}_K = \mathfrak{F}_b \mathbf{d}_{K,b}$ for aircraft nodes or $\mathbf{d}_K = \mathfrak{F}_0 \mathbf{d}_{K,0}$ for mount nodes, and by the Euler rotation vector $\boldsymbol{\varphi}_{K,b} = \left\{ \phi_{K,b} \quad \theta_{K,b} \quad \psi_{K,b} \right\}^T$ for aircraft nodes and $\boldsymbol{\varphi}_{K,0} = \left\{ \phi_{K,0} \quad \theta_{K,0} \quad \psi_{K,0} \right\}^T$ for mount nodes. Small deformations are assumed. Hence, as derived in Ref. [1], one obtains:

$$ \mathbf{d}_{OK,b} = \mathbf{d}_{K,b}, \tag{16} $$
$$ \mathbf{d}_{OK,0} = \mathbf{d}_{K,0}, \tag{17} $$
$$ \mathbf{d}_{KJ,b} = \widetilde{\boldsymbol{\varphi}_{K,b}}\mathbf{s}_{KJ,b}, \tag{18} $$
$$ \mathbf{d}_{KJ,0} = \widetilde{\boldsymbol{\varphi}_{K,0}}\mathbf{s}_{KJ,0}, \tag{19} $$
$$ \mathbf{d}_{JI,b} = \widetilde{\boldsymbol{\varphi}_{K,b}}\mathbf{s}_{JI,b}, \tag{20} $$
$$ \mathbf{d}_{JI,0} = \widetilde{\boldsymbol{\varphi}_{K,0}}\mathbf{s}_{JI,0}. \tag{21} $$

The nodal displacements and rotations, $\mathbf{d}_{K,b}$, $\boldsymbol{\varphi}_{K,b}$, $\mathbf{d}_{K,0}$ and $\boldsymbol{\varphi}_{K,0}$, can be recovered from the finite-element displacement vector, $\mathbf{u}_G$, with time-invariant Boolean matrices [1], $\mathbf{U}_{t,b,KG}$, $\mathbf{U}_{r,b,KG}$, $\mathbf{U}_{t,0,KG}$ and $\mathbf{U}_{r,0,KG}$, respectively:

$$ \mathbf{d}_{K,b} = \mathbf{U}_{t,b,KG}\mathbf{u}_G, \tag{22} $$
$$ \mathbf{d}_{K,0} = \mathbf{U}_{t,0,KG}\mathbf{u}_G, \tag{23} $$
$$ \boldsymbol{\varphi}_{K,b} = \mathbf{U}_{r,b,KG}\mathbf{u}_G, \tag{24} $$
$$ \boldsymbol{\varphi}_{K,0} = \mathbf{U}_{r,0,KG}\mathbf{u}_G. \tag{25} $$

Equations (7-8) and (15-25) yield:

$$ \mathbf{R}_I|_{acft} = \mathfrak{F}_b \left(\mathbf{R}_{O,b} + \mathbf{s}_{OI,b} + \left(\mathbf{U}_{t,b,KG} - \widetilde{\mathbf{s}_{KI,b}}\mathbf{U}_{r,b,KG} \right) \mathbf{u}_G \right), \tag{26} $$
$$ \mathbf{R}_I|_{mount} = \mathfrak{F}_0 \left(\mathbf{s}_{OI,0} + \left(\mathbf{U}_{t,0,KG} - \widetilde{\mathbf{s}_{KI,b}}\mathbf{U}_{r,0,KG} \right) \mathbf{u}_G \right), \tag{27} $$

$$ \begin{aligned} {}^{0}\dot{\mathbf{R}}_I\Big|_{acft} = \mathfrak{F}_b \Big({}^{b}\dot{\mathbf{R}}_{O,b} + \widetilde{\boldsymbol{\omega}_b}\mathbf{R}_{O,b} + \widetilde{\boldsymbol{\omega}_b}\mathbf{s}_{OI,b} + \left(\mathbf{U}_{t,b,KG} - \widetilde{\mathbf{s}_{KI,b}}\mathbf{U}_{r,b,KG} \right) \dot{\mathbf{u}}_G + \\ \widetilde{\boldsymbol{\omega}_b} \left(\mathbf{U}_{t,b,KG} - \widetilde{\mathbf{s}_{KI,b}}\mathbf{U}_{r,b,KG} \right) \mathbf{u}_G \Big), \end{aligned} \tag{28} $$
$$ {}^{0}\dot{\mathbf{R}}_I\Big|_{mount} = \mathfrak{F}_0 \left(\left(\mathbf{U}_{t,0,KG} - \widetilde{\mathbf{s}_{KI,0}}\mathbf{U}_{r,0,KG} \right) \dot{\mathbf{u}}_G \right). \tag{29} $$

The kinetic energy is calculated using the equation:

$$T = 1/2 \int_V {}^0\dot{\mathbf{R}}_I \cdot {}^0\dot{\mathbf{R}}_I \rho dV = 1/2 \sum_{j=1}^{N_m} \int_{V_j} {}^0\dot{\mathbf{R}}_I \cdot {}^0\dot{\mathbf{R}}_I \rho dV. \tag{30}$$

The point J is the CM of each sub-domain V_j and, then:

$$\int_{V_j} \mathbf{s}_{JI,b} \rho dV = \mathbf{0}. \tag{31}$$

With gravity assumed uniform over the airframe, the aircraft CM and center of gravity (CG) coincide, the reason why only the latter designation will be used henceforth. Calculating and summing the contributions of each sub-domain to the kinetic energy, and considering that $\mathbf{V}_b = {}^b\dot{\mathbf{R}}_{O,b} + \widetilde{\omega}_b \mathbf{R}_{O,b}$, the final expression for the kinetic energy becomes:

$$\begin{aligned} T = 1/2\, m_{acft} {\mathbf{V}_b}^T \mathbf{V}_b + 1/2\, {\omega_b}^T \left(\mathbf{J}_{O,acft} + \Delta\mathbf{J}_{O,acft}\right) \omega_b \\ -m_{acft} {\mathbf{V}_b}^T \left(\widetilde{\mathbf{s}_{CG,acft,b}} + \widetilde{\mathbf{d}_{CG,acft,b}}\right) \omega_b + m_{acft} {\mathbf{V}_b}^{Tb} \dot{\mathbf{d}}_{CG,acft,b} \\ +\dot{\mathbf{u}}_G^T \mathbf{M}_{\omega G}{}^T \omega_b + 1/2\, \dot{\mathbf{u}}_G^T \mathbf{M}_{GG} \dot{\mathbf{u}}_G \end{aligned} \tag{32}$$

with:

$$\mathbf{J}_{O,acft} = \frac{1}{2} \sum_{j=1}^{N_{m,acft}} \left(m_j \widetilde{\mathbf{s}_{OJ,b}}^T \widetilde{\mathbf{s}_{OJ,b}} + \mathbf{J}_j \right), \tag{33}$$

$$\begin{aligned} \Delta\mathbf{J}_{O,acft} = 2 \sum_{j=1}^{N_{m,acft}} m_j \left(\widetilde{\mathbf{s}_{OJ,b}}^T \widetilde{\mathbf{d}_{K,b}} + \widetilde{\mathbf{s}_{OK,b}}^T \mathbf{s}_{KJ,b} {\boldsymbol{\varphi}_{K,b}}^T - \widetilde{\mathbf{s}_{OJ,b}}^T \boldsymbol{\varphi}_{K,b} {\mathbf{s}_{KJ,b}}^T \right) \\ + \sum_{j=1}^{N_{m,acft}} m_j \left(\widetilde{\mathbf{d}_{K,b}}^T \widetilde{\mathbf{d}_{K,b}} + 2 \left(\widetilde{\mathbf{d}_{K,b}}^T \mathbf{s}_{KJ,b} {\boldsymbol{\varphi}_{K,b}}^T - \widetilde{\mathbf{d}_{K,b}}^T \boldsymbol{\varphi}_{K,b} {\mathbf{s}_{KJ,b}}^T \right) \right) \\ + \sum_{j=1}^{N_{m,acft}} \left(\left(m_j \widetilde{\mathbf{s}_{KJ,b}}^T \widetilde{\mathbf{s}_{KJ,b}} + \mathbf{J}_j \right) \boldsymbol{\varphi}_{K,b} {\boldsymbol{\varphi}_{K,b}}^T \right) \\ + \sum_{j=1}^{N_{m,acft}} \left(\widetilde{\boldsymbol{\varphi}_{K,b}} \left(2\mathbf{J}_j - \mathrm{tr}\left(\mathbf{J}_j\right) \mathbf{I}_3 - \widetilde{\boldsymbol{\varphi}_{K,b}} \left(m_j \mathbf{s}_{KJ,b} {\mathbf{s}_{KJ,b}}^T - \mathbf{J}_j + 1/2\ \mathrm{tr}\left(\mathbf{J}_j\right) \mathbf{I}_3 \right) \right) \right), \end{aligned} \tag{34}$$

$$\mathbf{M}_{GG} = \sum_{j=1}^{N_{m,acft}} m_j \left({\mathbf{U}_{t,b,KG}}^T \mathbf{U}_{t,b,KG} - {\mathbf{U}_{t,b,KG}}^T \widetilde{\mathbf{s}_{KJ,b}} \mathbf{U}_{r,b,KG} \right. \tag{35}$$

$$\left. - {\mathbf{U}_{r,b,KG}}^T {\widetilde{\mathbf{s}_{KJ,b}}}^T \mathbf{U}_{t,b,KG} \right) + \sum_{j=1}^{N_{m,acft}} {\mathbf{U}_{r,b,KG}}^T \left(m_j {\widetilde{\mathbf{s}_{KJ,b}}}^T \widetilde{\mathbf{s}_{KJ,b}} + \mathbf{J}_j \right) \mathbf{U}_{r,b,KG}$$

$$+ \sum_{j=N_{m,acft}+1}^{N_{m,acft}+N_{m,mount}} m_j \left({\mathbf{U}_{t,0,KG}}^T \mathbf{U}_{t,0,KG} - {\mathbf{U}_{t,0,KG}}^T \widetilde{\mathbf{s}_{KJ,0}} \mathbf{U}_{r,0,KG} \right.$$

$$\left. - {\mathbf{U}_{r,0,KG}}^T {\widetilde{\mathbf{s}_{KJ,0}}}^T \mathbf{U}_{t,0,KG} \right) + \sum_{j=N_{m,acft}+1}^{N_{m,acft}+N_{m,mount}} {\mathbf{U}_{r,0,KG}}^T \left(m_j {\widetilde{\mathbf{s}_{KJ,0}}}^T \widetilde{\mathbf{s}_{KJ,0}} + \mathbf{J}_j \right) \mathbf{U}_{r,0,KG},$$

$$\mathbf{s}_{CG,acft,b} = \frac{1}{m_{acft}} \sum_{j=1}^{N_{m,acft}} m_j \left(\mathbf{s}_{OK,b} + \mathbf{s}_{KJ,b} \right), \tag{36}$$

$$\mathbf{d}_{CG,acft,b} = \frac{1}{m_{acft}} \sum_{j=1}^{N_{m,acft}} m_j \left(\mathbf{U}_{t,b,KG} - \widetilde{\mathbf{s}_{KJ,b}} \mathbf{U}_{r,b,KG} \right) \mathbf{u}_G = \mathbf{D}_{CG,acft,b} \mathbf{u}_G, \tag{37}$$

$${\mathbf{M}_{\boldsymbol{\omega} G}}^T = - \sum_{j=1}^{N_{m,acft}} \left(m_j \left(\mathbf{U}_{t,b,KG} - \widetilde{\mathbf{s}_{KJ,b}} \mathbf{U}_{r,b,KG} \right)^T \widetilde{\mathbf{s}_{OJ,b}} - {\mathbf{U}_{r,b,KG}}^T \mathbf{J}_j \right) \tag{38}$$

$$- \sum_{j=1}^{N_{m,acft}} m_j \left(\mathbf{U}_{t,b,KG} - \widetilde{\mathbf{s}_{KJ,b}} \mathbf{U}_{r,b,KG} \right)^T \text{skew} \left(\mathbf{U}_{t,b,KG} \mathbf{u}_G - \widetilde{\mathbf{s}_{KJ,b}} \mathbf{U}_{r,b,KG} \mathbf{u}_G \right)$$

$$- \sum_{j=1}^{N_{m,acft}} {\mathbf{U}_{r,b,KG}}^T \left(\widetilde{\mathbf{U}_{r,b,KG} \mathbf{u}_G} \left(-\mathbf{J}_j + 1/2 \ \text{tr} \left(\mathbf{J}_j \right) \mathbf{I}_3 \right) \right)$$

$$= {\overline{\mathbf{M}_{\boldsymbol{\omega} G}}}^T + {\Delta \mathbf{M}_{\boldsymbol{\omega} G}}^T,$$

and $\mathbf{J}_j$ the inertia matrix of the jth lumped-mass element about its own center of mass.

The elastic strain energy for the aeroelastic system structure modeled with finite elements reads:

$$U_{elas} = 1/2 \left(\mathbf{T}_{FEM|BRF} \mathbf{u}_G \right)^T \mathbf{K}_{FEM} \left(\mathbf{T}_{FEM|BRF} \mathbf{u}_G \right) = 1/2 \ {\mathbf{u}_G}^T \mathbf{K}_{GG} \mathbf{u}_G, \tag{39}$$

where the FEM model nodal displacements can be calculated in generic coordinate systems other than the flight-mechanics BRF coordinate system. The three-dimensional transformation matrices from the BRF to such coordinate systems are collected in the block-diagonal transformation matrix $\mathbf{T}_{FEM|BRF}$, such that the original FEM stiffness matrix, $\mathbf{K}_{FEM}$, is transformed to $\mathbf{K}_{GG} = {\mathbf{T}_{FEM|BRF}}^T \mathbf{K}_{FEM} \mathbf{T}_{FEM|BRF}$.

The gravitational potential energy is given by:

$$U_{grav} = -\sum_{j=1}^{N_m} \int_{V_j} \mathbf{g} \cdot \mathbf{R}_I \rho dV \tag{40}$$
$$= -m_{acft}\mathbf{g}_b{}^T \left(\mathbf{R}_{O,b} + \mathbf{s}_{CG,acft,b} + \mathbf{d}_{CG,acft,b}\right) - m_{mount}\mathbf{g}_0{}^T \left(\mathbf{s}_{CG,mount,0} + \mathbf{d}_{CG,mount,0}\right),$$

where:

$$\mathbf{s}_{CG,mount,0} = \frac{1}{m_{mount}} \sum_{j=N_{m,acft}+1}^{N_{m,acft}+N_{m,mount}} m_j \left(\mathbf{s}_{OK,0} + \mathbf{s}_{KJ,0}\right), \tag{41}$$

$$\mathbf{d}_{CG,mount,0} = \frac{1}{m_{mount}} \sum_{j=N_{m,acft}+1}^{N_{m,acft}+N_{m,mount}} m_j \left(\mathbf{U}_{t,0,KG} - \widetilde{\mathbf{s}_{KJ,0}}\mathbf{U}_{r,0,KG}\right) \mathbf{u}_G = \mathbf{D}_{CG,mount,0}\mathbf{u}_G, \tag{42}$$

At last, structural dissipation due to damping forces of viscous nature is assumed [30]:

$$\mathcal{F} = 1/2\ \dot{\mathbf{u}}_G^T \mathbf{B}_{GG} \dot{\mathbf{u}}_G. \tag{43}$$

2.1 Constraints

Six of the constraints to which the aeroelastic system is subjected correspond to the clamp of the flexible mount to the wind-tunnel wall. Such constraints can be expressed by the equation:

$$\mathbf{u}_{c,mount,0} = \mathbf{U}_{c,mount}^T \mathbf{u}_G = \mathbf{0}, \tag{44}$$

where $\mathbf{U}_{c,mount} \in \mathbb{R}^{n,6}$ is the Boolean matrix that selects the structural clamp degrees of freedom from the complete set of DOFs.

Additionally, the aircraft structure is considered to be clamped at the structural node that coincides in position with the mount node connected to the aircraft, resulting in other six constraints:

$$\mathbf{u}_{c,acft,b} = \mathbf{U}_{c,acft}^T \mathbf{u}_G = \mathbf{0}, \tag{45}$$

with $\mathbf{U}_{c,acft} \in \mathbb{R}^{n,6}$.

The degrees of freedom of the node at the other end of the mount, where the connection to the aircraft is located, are given by the vector $\mathbf{u}_{con,mount,0} = \mathbf{U}_{con,mount}^T \mathbf{u}_G$. Therefore, the translational holonomic constraints for the aircraft are represented by the equations:

$$\mathbf{R}_{O,b}\left(t\right)=\mathbf{C}_{b0}\left(t\right)\left(\mathbf{s}_{con,mount,0}+{\mathbf{U}_{t,con,mount}}^{T}\mathbf{u}_{G}\right), \tag{46}$$

where $\mathbf{s}_{con,mount,0}$ is the position vector of the mount node at the aircraft-mount connection in the undeformed condition, and ${\mathbf{U}_{t,con,mount}}^{T}$ is the Boolean matrix giving the translational displacements of the same node.

Any of the rotational degrees of freedom of the body reference frame, given by the Euler angles, can also be constrained. These correspond to n_c-3 constraints.

The first fifteen constraints of the aeroelastic system can be summarized by the equation $\mathbf{F}_{15}\left(\mathbf{q},t\right)=\mathbf{0}$, where $\mathbf{F}_{15}\left(\mathbf{q},t\right)$ is given by:

$$\mathbf{F}_{15}\left(\mathbf{q},t\right)=\begin{bmatrix}{\mathbf{U}_{c,mount}}^{T}\mathbf{u}_{G}\left(t\right)\\{\mathbf{U}_{c,acft}}^{T}\mathbf{u}_{G}\left(t\right)\\\mathbf{R}_{O,b}\left(t\right)-\mathbf{C}_{b0}\left(t\right)\left(\mathbf{s}_{con,mount,0}+{\mathbf{U}_{t,con,mount}}^{T}\mathbf{u}_{G}\left(t\right)\right)\end{bmatrix}. \tag{47}$$

The additional n_c-3 constraints can be summarized by:

$$\mathbf{F}_{n_c-3}\left(\mathbf{q},t\right)=\begin{cases}m_{\phi}\left(\phi\left(t\right)-\phi_c-{\mathbf{e}_{3,1}}^{T}{\mathbf{U}_{r,con,mount}}^{T}\mathbf{u}_{G}\left(t\right)\right),\ k=m_{\phi},\\m_{\theta}\left(\theta\left(t\right)-\theta_c-{\mathbf{e}_{3,2}}^{T}{\mathbf{U}_{r,con,mount}}^{T}\mathbf{u}_{G}\left(t\right)\right),\ k=m_{\phi}+m_{\theta},\\m_{\psi}\left(\psi\left(t\right)-\psi_c-{\mathbf{e}_{3,3}}^{T}{\mathbf{U}_{r,con,mount}}^{T}\mathbf{u}_{G}\left(t\right)\right),\ k=m_{\phi}+m_{\theta}+m_{\psi},\end{cases} \tag{48}$$

where m_{ϕ}, m_{θ}, and m_{ψ} are 1 if the constraint is active and 0 if the constraint is inactive; ϕ_c, θ_c and ψ_c are the values at which the corresponding angles are constrained in addition to the elastic rotational twist of the mount tip; and ${\mathbf{U}_{r,con,mount}}^{T}$ is the Boolean matrix giving the rotational displacements about the inertial axes of the structural node at the end of the mount to which the aircraft is connected.

The whole set of holonomic constraints can be written in matrix form:

$$\mathbf{F}_{12+n_c}\left(\mathbf{q},t\right)=\begin{bmatrix}\mathbf{F}_{15}\left(\mathbf{q},t\right)\\\mathbf{F}_{n_c-3}\left(\mathbf{q},t\right)\end{bmatrix}. \tag{49}$$

Considering Lagrange's equations, Eq. (4), the following relations become useful:

$$\frac{\partial\mathbf{F}_{12+n_c}}{\partial\mathbf{R}_{O,b}}=\begin{bmatrix}\mathbf{0}_{12\times3}\\\mathbf{I}_{3}\\\mathbf{0}_{n_c-3\times3}\end{bmatrix}, \tag{50}$$

$$\frac{\partial\mathbf{F}_{12+n_c}}{\partial\boldsymbol{\varphi}}=\begin{bmatrix}\mathbf{0}_{12\times3}\\-\widetilde{\mathbf{R}_{O,b}}\left({\mathbf{H}_{\boldsymbol{\varphi}}}^{-1}\right)\\m_{\phi}\mathbf{e}_{n_c-3,m_{\phi}}{\mathbf{e}_{3,1}}^{T}+m_{\theta}\mathbf{e}_{n_c-3,m_{\phi}+m_{\theta}}{\mathbf{e}_{3,2}}^{T}+\\+m_{\psi}\mathbf{e}_{n_c-3,m_{\phi}+m_{\theta}+m_{\psi}}{\mathbf{e}_{3,3}}^{T}\end{bmatrix}=\begin{bmatrix}\mathbf{0}_{12\times3}\\-\widetilde{\mathbf{R}_{O,b}}\left({\mathbf{H}_{\boldsymbol{\varphi}}}^{-1}\right)\\\mathbf{M}_{\phi\theta\psi}\end{bmatrix}, \tag{51}$$

$$\frac{\partial \mathbf{F}_{12+n_c}}{\partial \mathbf{u}_G} = \begin{bmatrix} \mathbf{U}_{c,mount}{}^T \\ \mathbf{U}_{c,acft}{}^T \\ -\mathbf{C}_{b0}\left(t\right)\mathbf{U}_{t,con,mount}{}^T \\ -m_\phi \mathbf{e}_{n_c-3,m_\phi}\mathbf{e}_{3,1}{}^T\mathbf{U}_{r,con,mount}{}^T - m_\theta \mathbf{e}_{n_c-3,m_\phi+m_\theta}\mathbf{e}_{3,2}{}^T\mathbf{U}_{r,con,mount}{}^T + \\ -m_\psi \mathbf{e}_{n_c-3,m_\phi+m_\theta+m_\psi}\mathbf{e}_{3,3}{}^T\mathbf{U}_{r,con,mount}{}^T \end{bmatrix}, \quad (52)$$

where $\mathbf{e}_{N,i}$ denotes a column matrix with N entries of which the ith is equal to 1 and all the others are null, and the notation $\frac{\partial \mathbf{f}}{\partial \mathbf{x}}$ is such that $\mathbf{e}_{n_f,i}{}^T\frac{\partial \mathbf{f}}{\partial \mathbf{x}}\mathbf{e}_{n_x,j} = \frac{\partial f_i}{\partial x_j}$, with n_f the number of elements of $\mathbf{f}$ and n_x the number of elements of $\mathbf{x}$.

The right-hand side of Eq. (4) can then be represented by:

$$\sum_{k=1}^{12+n_c} \lambda_k \frac{\partial f_k}{\partial q_i} + Q_i = \frac{\partial \mathbf{F}_{12+n_c}}{\partial q_i}{}^T \mathbf{\Lambda} + Q_i = Q_{c,i} + Q_i, \quad (53)$$

where $Q_{c,i} = \partial \mathbf{F}_{12+n_c}/\partial q_i{}^T \mathbf{\Lambda}$ is the generalized constraint reaction on the q_i degree of freedom, and $\mathbf{e}_{12+n_c,k}\mathbf{\Lambda} = \lambda_k$. In the next section, the generalized forces Q_i are derived.

2.2 Generalized Forces

The aerodynamic forces acting on the wind-tunnel mount will be neglected in this paper. Thus, the generalized forces, comprising the aerodynamic and the propulsive forces of the aircraft, are calculated with the equation [30]:

$$Q_i = \int_{VA} \mathbf{f}_I \cdot \frac{\partial \mathbf{R}_I}{\partial q_i} dV = \int_{VA} \mathbf{f}_{I,b}{}^T \mathfrak{F}_b{}^T \left(\frac{\partial \mathfrak{F}_b}{\partial q_i}\mathbf{R}_{I,b} + \mathfrak{F}_b \frac{\partial \mathbf{R}_{I,b}}{\partial q_i} \right) dV, \quad (54)$$

where $\mathbf{f}_I$ is the force vector per unit volume acting on the generic point I in the aircraft.

The propulsive forces can be modeled as concentrated thrust forces acting on the thrust center of each one of the N_E aircraft engines. Considering that a matrix $\mathbf{C}_{be}$ transforms the thrust force from an engine frame – whose x axis is aligned with the thrust line – to the body frame, one has the concentrated force $\mathbf{T}_{e,b} = \mathbf{C}_{be}\mathbf{e}_{3,1}T_e$ applied at a point E whose position vector with respect to O in the undeformed aircraft is $\mathbf{s}_{OE,b}$.

Every thrust center is also considered to be coincident with or rigidly connected to a structural node K_E in the FEM model of the aircraft, with associated Boolean matrices $\mathbf{U}_{t,b,K_EG}$ and $\mathbf{U}_{r,b,K_EG}$. The translations and the rotations of the thrust center are then given by the vectors $\mathbf{d}_{e,b} = \left(\mathbf{U}_{t,b,K_EG} - \widetilde{\mathbf{s}_{K_EE,b}}\mathbf{U}_{r,b,K_EG}\right)\mathbf{u}_G$ and $\boldsymbol{\varphi}_e = \mathbf{U}_{r,b,K_EG}\mathbf{u}_G$, respectively, with $\mathbf{s}_{K_EE,b}$ the position vector of the thrust center with respect to K_E.

Under small deformations, the thrust vector is $\mathbf{T}_{e,b} = \left(\mathbf{C}_{be} + \widetilde{\boldsymbol{\varphi}_e}\right)\mathbf{e}_{3,1}T_e$ and the thrust center is $\mathbf{s}_{OE,b} + \mathbf{d}_{e,b}$. The concentrated propulsive force can be represented as a distributed force by means of a three-dimensional Dirac's delta function [16]. As a result, the final expressions for the generalized forces in the BRF DOFs become:

$$\mathbf{Q}_{\mathbf{R}_{O,b}} = \mathbf{F}_{a,b} + \sum_{e=1}^{N_E} \mathbf{C}_{be} T_e \mathbf{e}_{3,1} + \Delta\mathbf{F}_{a,b} + \sum_{e=1}^{N_E} \widetilde{\boldsymbol{\varphi}_e} T_e \mathbf{e}_{3,1} = \mathbf{F}_b + \Delta\mathbf{F}_b, \tag{55}$$

$$\begin{aligned}\mathbf{Q}_{\boldsymbol{\varphi}} &= \left(\mathbf{H}_{\boldsymbol{\varphi}}{}^{-1}\right)^T \left(\mathbf{M}_{a,O,b} + \sum_{e=1}^{N_E} \widetilde{\mathbf{s}_{OE,b}} T_e \mathbf{C}_{be} \mathbf{e}_{3,1} + \Delta\mathbf{M}_{a,O,b} + \Delta\mathbf{M}_{p,O,b} + \widetilde{\mathbf{R}_{O,b}} \mathbf{Q}_{\mathbf{R}_{O,b}} \right) \\ &= \left(\mathbf{H}_{\boldsymbol{\varphi}}{}^{-1}\right)^T \left(\mathbf{M}_{O,b} + \Delta\mathbf{M}_{O,b} + \widetilde{\mathbf{R}_{O,b}} \left(\mathbf{F}_b + \Delta\mathbf{F}_b\right) \right),\end{aligned} \tag{56}$$

where $\mathbf{F}_{a,b}$ and $\mathbf{M}_{a,O,b}$ are the net aerodynamic force and moment vectors, respectively, associated with the rigid airframe; $\Delta\mathbf{F}_{a,b}$ and $\Delta\mathbf{M}_{a,O,b}$ are the net incremental aerodynamic force and moment vectors, respectively, due to the elastic motion; and:

$$\Delta\mathbf{M}_{p,O,b} = \sum_{e=1}^{N_E} T_e \left(\widetilde{\mathbf{s}_{OE,b}} (\widetilde{\mathbf{U}_{r,b,K_EG}} \mathbf{u}_G) + \text{skew}\left(\left(\mathbf{U}_{t,b,K_EG} - \widetilde{\mathbf{s}_{K_EE,b}} \mathbf{U}_{r,b,K_EG} \right) \mathbf{u}_G \right) \mathbf{C}_{be} \right) \mathbf{e}_{3,1}$$

is the net linearized incremental propulsive moment vector due to the structural displacements. All the moments are about O.

The aerodynamic forces can be simplified with the use of lifting-surface methods like the vortex-lattice method (VLM) [31] and the doublet-lattice method (DLM) [25]. Hence, the aerodynamic forces and moments are concentrated on a discrete set of N_P aerodynamic grid points, located at the centroids of the VLM/DLM boxes, with N_P equal to the number of boxes in the discretization of the aerodynamic model. The structural displacements at the aerodynamic grid points are calculated with a linear transformation matrix $\mathbf{G}_{AG}$ that provides the vector of aerodynamic normal and rotational displacements, $\mathbf{u}_A$, from the structural displacements, $\mathbf{u}_G$: $\mathbf{u}_A = \mathbf{G}_{AG}\mathbf{u}_G$. Each aerodynamic grid point has two degrees of freedom – plunge and pitch – and the length N_A of the $\mathbf{u}_A$ vector is then $N_A = 2N_P$. The vector containing the aerodynamic forces and moments at the aerodynamic grid points is $\mathbf{P}_A$. With this rationale and based on Eq. (54), the generalized force in each $u_g = \mathbf{e}_{n,g}{}^T \mathbf{u}_G$ DOF reads:

$$\begin{aligned} Q_g &= \mathbf{e}_{n,g}{}^T \mathbf{G}_{AG}{}^T \mathbf{P}_A \\ &+ \mathbf{e}_{n,g}{}^T \sum_{e=1}^{N_E} \left(\mathbf{U}_{t,b,K_EG} - \widetilde{\mathbf{s}_{K_EE,b}} \mathbf{U}_{r,b,K_EG} \right)^T T_e \left(\mathbf{C}_{be} \mathbf{e}_{3,1} - \widetilde{\mathbf{e}_{3,1}} \mathbf{U}_{r,b,K_EG} \mathbf{u}_G \right), \end{aligned} \tag{57}$$

and each Q_g can be collected in a vector $\mathbf{Q}_G = \sum_{g=1}^{n} \mathbf{e}_{n,g} Q_g$ respecting the ordering of $\mathbf{u}_G$:

$$\mathbf{Q}_G = \mathbf{G}_{AG}{}^T \mathbf{P}_A + \sum_{e=1}^{N_E} \left(\mathbf{U}_{t,b,K_EG} - \widetilde{\mathbf{s}_{K_EE,b}} \mathbf{U}_{r,b,K_EG} \right)^T T_e \left(\mathbf{C}_{be} \mathbf{e}_{3,1} - \widetilde{\mathbf{e}_{3,1}} \mathbf{U}_{r,b,K_EG} \mathbf{u}_G \right) \tag{58}$$

2.3 Equations of Motion

The equations of motion for the constrained flexible aircraft can be obtained by the substitution of the energy expressions, Eqs. (32), (39) and (40); Rayleigh's dissipation function, Eq. (43); the holonomic constraints' partial derivatives, Eqs. (50), (51), and (52); and the generalized forces, Eqs. (55), (56) and (58), into Lagrange's equations, Eq. (4). It is assumed in the derivation that no change in the aircraft mass occurs with time. The EOMs then read:

$$
\begin{aligned}
&m_{acft}\dot{\mathbf{V}}_b + m_{acft}\widetilde{\boldsymbol{\omega}_b}\mathbf{V}_b - m_{acft}\widetilde{\mathbf{s}_{CG,acft,b}}\dot{\boldsymbol{\omega}}_b - m_{acft}\widetilde{\boldsymbol{\omega}_b}\widetilde{\mathbf{s}_{CG,acft,b}}\boldsymbol{\omega}_b \\
&+m_{acft}\widetilde{\dot{\boldsymbol{\omega}}_b}\mathbf{D}_{CG,acft,b}\mathbf{u}_G + 2m_{acft}\widetilde{\boldsymbol{\omega}_b}\mathbf{D}_{CG,acft,b}\dot{\mathbf{u}}_G \\
&+m_{acft}\widetilde{\boldsymbol{\omega}_b}\widetilde{\boldsymbol{\omega}_b}\mathbf{D}_{CG,acft,b}\mathbf{u}_G + m_{acft}\mathbf{D}_{CG,acft,b}\ddot{\mathbf{u}}_G \\
&= m_{acft}\mathbf{g}_b + \mathbf{F}_b + \Delta\mathbf{F}_b + \begin{Bmatrix}\lambda_{13} & \lambda_{14} & \lambda_{15}\end{Bmatrix}^T,
\end{aligned}
\tag{59}
$$

$$
\begin{aligned}
&\mathbf{J}_{O,acft}\dot{\boldsymbol{\omega}}_b + \widetilde{\boldsymbol{\omega}_b}\mathbf{J}_{O,acft}\boldsymbol{\omega}_b + m_{acft}\widetilde{\mathbf{s}_{CG,acft,b}}\left(\dot{\mathbf{V}}_b + \widetilde{\boldsymbol{\omega}_b}\mathbf{V}_b\right) \\
&+m_{acft}\widetilde{\mathbf{D}_{CG,acft,b}\mathbf{u}_G}\left(\dot{\mathbf{V}}_b + \widetilde{\boldsymbol{\omega}_b}\mathbf{V}_b\right) \\
&+\Delta\mathbf{J}'_{O,acft}\dot{\boldsymbol{\omega}}_b + \widetilde{\boldsymbol{\omega}_b}\Delta\mathbf{J}'_{O,acft}\boldsymbol{\omega}_b + \Delta\dot{\mathbf{J}}'_{O,acft}\boldsymbol{\omega}_b + \dot{\mathbf{M}}_{\boldsymbol{\omega}G}\dot{\mathbf{u}}_G + \mathbf{M}_{\boldsymbol{\omega}G}\ddot{\mathbf{u}}_G + \widetilde{\boldsymbol{\omega}_b}\mathbf{M}_{\boldsymbol{\omega}G}\dot{\mathbf{u}}_G \\
&= m_{acft}\widetilde{\mathbf{s}_{CG,acft,b}}\mathbf{g}_b + m_{acft}\widetilde{\mathbf{D}_{CG,acft,b}\mathbf{u}_G}\mathbf{g}_b + \mathbf{M}_{O,b} + \Delta\mathbf{M}_{O,b} \\
&+{\mathbf{H}_{\boldsymbol{\varphi}}}^T\left(m_\phi\mathbf{e}_{3,1}\lambda_{15+m_\phi} + m_\theta\mathbf{e}_{3,2}\lambda_{15+m_\phi+m_\theta} + m_\psi\mathbf{e}_{3,3}\lambda_{15+m_\phi+m_\theta+m_\psi}\right),
\end{aligned}
\tag{60}
$$

$$
\begin{aligned}
&\mathbf{M}_{GG}\ddot{\mathbf{u}}_G + \mathbf{B}_{GG}\dot{\mathbf{u}}_G + \mathbf{K}_{GG}\mathbf{u}_G \\
&+m_{acft}{\mathbf{D}_{CG,acft,b}}^T\left(\dot{\mathbf{V}}_b + \widetilde{\boldsymbol{\omega}_b}\mathbf{V}_b\right) + {\mathbf{M}_{\boldsymbol{\omega}G}}^T\dot{\boldsymbol{\omega}}_b \\
&+2\dot{\mathbf{M}}^T_{\boldsymbol{\omega}G}\boldsymbol{\omega}_b - \frac{1}{2}\sum_{g=1}^{n}\mathbf{e}_{n,g}{\boldsymbol{\omega}_b}^T\frac{\partial\Delta\mathbf{J}_{O,acft}}{\partial u_g}\boldsymbol{\omega}_b \\
&= m_{acft}{\mathbf{D}_{CG,acft,b}}^T\mathbf{g}_b + m_{mount}{\mathbf{D}_{CG,mount,0}}^T\mathbf{g}_0 + \mathbf{Q}_G \\
&+\mathbf{U}_{c,mount}\begin{Bmatrix}\lambda_1 & \lambda_2 & \lambda_3 & \lambda_4 & \lambda_5 & \lambda_6\end{Bmatrix}^T \\
&+\mathbf{U}_{c,acft}\begin{Bmatrix}\lambda_7 & \lambda_8 & \lambda_9 & \lambda_{10} & \lambda_{11} & \lambda_{12}\end{Bmatrix}^T - \mathbf{U}_{t,con,mount}{\mathbf{C}_{b0}}^T\begin{Bmatrix}\lambda_{13} & \lambda_{14} & \lambda_{15}\end{Bmatrix}^T \\
&-\mathbf{U}_{r,con,mount}\left(m_\phi\mathbf{e}_{3,1}\lambda_{15+m_\phi} + m_\theta\mathbf{e}_{3,2}\lambda_{15+m_\phi+m_\theta} + m_\psi\mathbf{e}_{3,3}\lambda_{15+m_\phi+m_\theta+m_\psi}\right),
\end{aligned}
\tag{61}
$$

with $\Delta\mathbf{J}'_{O,acft} = 1/2\ \left(\Delta\mathbf{J}_{O,acft} + {\Delta\mathbf{J}_{O,acft}}^T\right)$ being the symmetric inertia matrix increment, and with all the time derivatives taken in the BRF (the left superscript b was omitted for brevity). Moreover, the equations of motion are also subjected to the constraints of Eqs. (47) and (48), so that the number of equations and unknowns match, allowing the calculation of the Lagrange multipliers.

2.4 Use of Modes of Vibration as Shape Functions

The modal superposition technique is generally a valid practical approach to solve dynamic problems involving the deformation of structures [30]. Mode shapes obtained from the undamped, linearized and conservative system can then be applied as shape functions in the solution of the structural-dynamic problem of the constrained aeroelastic aircraft. In the present study, it is proposed that the elastic disturbances around the equilibrium condition are represented by a superposition of the aeroelastic system modes of vibration, $\Delta\mathbf{u}_G = \mathbf{\Phi}\boldsymbol{\eta}$.

Different modal bases can be used for the aircraft and for the flexible mount. Since the latter is assumed to be clamped at its root, its modal basis consistently corresponds to a selected set of constrained modes of vibration. On the other hand, the aircraft structure would have in fact $n_c \leq 6$ constrained rigid-body DOFs at its connection to the mount. Hence, the modal basis for the aircraft structure may consist of the corresponding inertia-relieved constrained modes of vibration [1], with the inertia relief matrix calculated using only the unconstrained rigid-body modes of the aircraft structure. The consideration of inertia relief ensures that no support reaction will develop on unconstrained rigid-body DOFs [1].

2.5 Aerodynamic Model

The aerodynamic loads acting on the flexible aircraft can be calculated as the superposition of loads that would be obtained were the airframe perfectly rigid with incremental loads due to the structural deformation. In this case, the aerodynamic data for the rigid aircraft consists of tables of non-dimensional force and moment coefficients and do not comprise any structural flexibility effect. To obtain the generalized aerodynamic loads related to the structural motion, the VLM [31] and the DLM [25] are used in this paper, yielding the following linear system of equations:

$$\mathbf{A}^{-1}(\kappa)\Delta\mathbf{C}_\mathbf{p} = \mathbf{w}, \tag{62}$$

where $\mathbf{w} \in \mathbb{C}^{N_P}$ is the vector of non-dimensional normalwashes at the N_P panel control points; $\Delta\mathbf{C}_\mathbf{p} \in \mathbb{C}^{N_P}$ is the vector of panel pressure coefficient differences; and $\mathbf{A} \in \mathbb{C}^{N_P \times N_P}$ is the AIC (aerodynamic influence coefficient) matrix. The AIC matrix is dependent upon the reduced frequency, κ, and the geometry and discretization of the aerodynamic lifting surfaces in the model. Dependence on the Mach number, M, is neglected in this paper, since compressibility effects are not present in the cases studied here.

To allow linearized boundary-layer effects to be approximated in the incremental aerodynamic formulation, correction methods [34–36] can be applied to modify the AIC matrix, yielding a modified matrix $\mathbf{A}'$:

$$\Delta\mathbf{C}_\mathbf{p} = \mathbf{A}'(\kappa)\mathbf{w}. \tag{63}$$

The body frame of reference used to calculate the aerodynamic loads is defined as an aerodynamic reference frame (ARF). Its inertial angular rates are written in the ARF coordinate system

as p_a, q_a, and r_a, and its inertial velocity has the components u_a, v_a, and w_a in the same system [1]. The rigid-body motion of the aircraft then contributes to the generalized aerodynamic forces (GAFs) in the elastic DOFs in terms of p_a, q_a, r_a, u_a, v_a, w_a, the control surface deflections and other possible rigid-body variables. The elastic deformation of the structure measured with respect to the ARF, given by the vector $\mathbf{u}_{G/A}$, contributes to the incremental GAFs. The total GAFs are then given by [1]:

$$\mathbf{Q}_G = \bar{q}\mathbf{G}_{AG}{}^T\mathbf{S}_{AP}\left(\Delta\mathbf{C}_{\mathbf{p},\mathbf{u}} + \Delta\mathbf{C}_{\mathbf{p},\mathbf{e}}\right). \tag{64}$$

In Eq. (64), $\bar{q}$ is the dynamic pressure; $\mathbf{G}_{AG} \in \mathbb{R}^{N_A \times n}$ is the matrix that interpolates the elastic displacements from the structural nodes to the aerodynamic grid points (at the centroids of the VLM/DLM boxes); $\mathbf{S}_{AP} \in \mathbb{R}^{N_A \times N_P}$ transforms the panel pressure coefficient differences to forces and moments at the aerodynamic grid points, and is usually called an integration matrix; $\Delta\mathbf{C}_{\mathbf{p},\mathbf{u}}$ is the vector of panel pressure coefficient differences related to the rigid-body states, without elastic deformation; and $\Delta\mathbf{C}_{\mathbf{p},\mathbf{e}}$ is the vector of panel incremental pressure coefficient differences.

The problem hidden in Eqs. (63) and (64) is that the former is written in the frequency domain and the latter contains pressure coefficient difference distributions, $\Delta\mathbf{C}_{\mathbf{p},\mathbf{u}}$ and $\Delta\mathbf{C}_{\mathbf{p},\mathbf{e}}$, already in the time domain. Hence, a transformation from the frequency to the time domain is implicit. As in [22], the multiple-pole rational-function approximation (RFA) proposed by Eversman and Tewari [24] can be performed. In the frequency domain, one has [22]:

$$\Delta\mathbf{C}_{\mathbf{p},\mathbf{e}} = \mathbf{A}'\left(\kappa\right)\left(\mathbf{D}_{PA,0} + \mathrm{i}\kappa\mathbf{D}_{PA,1}\right)\mathbf{G}_{AG}\mathbf{u}_{G/A}, \tag{65}$$

with $\mathbf{D}_{PA,0}, \mathbf{D}_{PA,1} \in \mathbb{R}^{N_P \times N_A}$ the differentiation matrices that allow the calculation of control point normalwashes at three quarters of the boxes' mean chords from the displacements at the aerodynamic grid points, respectively; and $N_A = 2N_P$ is the total number of aerodynamic degrees of freedom (each panel has two DOFs, plunge and pitch). In the special case where the correction method corresponds to a left-multiplying correction matrix, $\mathbf{W}_{PP}$, independent of the reduced frequency, one has the following frequency-dependent term in Eq. (65):

$$\mathbf{Q}_{PG} = \mathbf{A}\left(\kappa\right)\left(\mathbf{D}_{PA,0} + \mathrm{i}\kappa\mathbf{D}_{PA,1}\right)\mathbf{G}_{AG}. \tag{66}$$

If the matrix $\mathbf{Q}_{PG}$ is approximated by rational functions and then written in the time domain, one can left-multiply it by $\mathbf{W}_{PP}$ to obtain the corresponding corrected pressure coefficient difference distribution. Hence, in the RFA, $\mathbf{Q}_{PG}$ is approximated as a rational function $\mathbf{Q}_{PG,ap}$ with zero-, first- and second-order terms, and a series of N_L real poles β_ℓ of multiplicity E_ℓ belonging to the left semi-plan, representing the aerodynamic lag effect caused by the flow unsteadiness:

$$\mathbf{Q}_{PG,ap}\left(\mathrm{i}\kappa\right) = \sum_{j=0}^{2}\mathbf{Q}_{PG(j)}(\mathrm{i}\kappa)^j + \sum_{\ell=1}^{N_L}\sum_{e=1}^{E_\ell}\mathbf{Q}_{PG(2+E_0+\ldots+E_{\ell-1}+e)}\left(\frac{\mathrm{i}\kappa}{\mathrm{i}\kappa+\beta_\ell}\right)^e, \tag{67}$$

with $\mathbf{Q}_{PG(i)} \in \mathbb{R}^{n\times n}$ the approximant matrices, still to be determined; and $E_0 = 0$. Eversman and Tewari [24] did not include the multiplication of each lag term by $(i\kappa)^e$ in their RFA, but this is done in this paper to keep a stronger analogy with Roger's RFA method [37] and so that the approximate static generalized aerodynamic matrix becomes directly equal to $\mathbf{Q}_{PG(0)}$.

The unavailable $\mathbf{Q}_{PG,ap}(s)$ matrix in the Laplace variable $s = \sigma + i\omega$ can be assumed analytic for a causal, stable, and linear system [24]. In this case, the analytic continuation principle can be used to express $\mathbf{Q}_{GG,ap}(s)$ as $\mathbf{Q}_{GG,ap}(i\omega)$ with the appropriate replacement of $i\omega$ by s. Then, using inverse Laplace transform, it can then be demonstrated that the corrected incremental pressure coefficient difference distribution in the time domain is:

$$\Delta\mathbf{C}_{\mathbf{p},\mathbf{e}} = \mathbf{W}_{PP}\left(\sum_{j=0}^{2}\mathbf{Q}_{PG(j)}\left(\frac{b_w}{V}\right)^j\frac{d^j\mathbf{u}_G}{dt^j} + \sum_{\ell=1}^{N_L}\sum_{e=1}^{E_\ell}\mathbf{Q}_{PG(2+E_0+\ldots+E_{\ell-1}+e)}\mathbf{u}_{lag(E_0+\ldots+E_{\ell-1}+e)}\right), \tag{68}$$

with:

$$\dot{\mathbf{u}}_{lag(E_0+\ldots+E_{\ell-1}+e)} = \dot{\mathbf{u}}_G - (V/b_w)\,\beta_\ell\sum_{\varepsilon=1}^{e}\mathbf{u}_{lag(E_0+\ldots+E_{\ell-1}+\varepsilon)},\ \ell = 1,\cdots,N_L. \tag{69}$$

Therefore, the representation of the aerodynamic lag by the RFA results in an augmentation of the system with $n\sum_{\ell=1}^{N_L}E_\ell$ states, showing the importance of keeping the quantity and the order of the lag parameters at a minimum. This implies a trade-off between the system complexity and the approximation quality.

To determine the approximant matrices $\mathbf{Q}_{PG(i)} \in \mathbb{R}^{n\times n}$ as a function of the selected set of lag parameters, β_ℓ, and their corresponding multiplicities, E_ℓ, a least-squares procedure is used, which is detailed in Ref. [22]. The solution of the least-squares problem is achieved by specifying the set of values of β_ℓ and E_ℓ. Since the least-squares procedure assures that the error is the minimum for the set of specified lag parameters and multiplicities, but not a global minimum, these nonlinear parameters shall be included as design variables in nonlinear optimization procedures [24].

The integration and differentiation matrices in Eq. (65) are given by:

$$\mathbf{S}_{AP} = \sum_{k=1}^{N_P} S_k\left(\mathbf{e}_{N_A,2k-1}\mathbf{e}_{N_P,k}{}^T + \mathbf{e}_{N_A,2k}\mathbf{e}_{N_P,k}{}^T\left(x_{050,k} - x_{025,k}\right)\right), \tag{70}$$

$$\mathbf{D}_{PA,0} = \sum_{k=1}^{N_P}\mathbf{e}_{N_P,k}\mathbf{e}_{N_A,2k}{}^T, \tag{71}$$

$$\mathbf{D}_{PA,1} = \frac{1}{b_w}\sum_{k=1}^{N_P}\left(\mathbf{e}_{N_P,k}\mathbf{e}_{N_A,2k-1}{}^T + \mathbf{e}_{N_P,k}\mathbf{e}_{N_A,2k}{}^T\left(x_{075,k} - x_{025,k}\right)\right), \tag{72}$$

with $x_{025,k}, x_{050,k}, x_{075,k}$ the x coordinates, in the aerodynamic model coordinate system, of the points at one quarter, one half and three quarters of the kth aerodynamic box (panel) mean chord; and S_k the kth aerodynamic box area.

In this paper, the aerodynamic reference frame is modeled with attached axes [1]. This means that the origin A is coincident with or rigidly connected to a material point C that remains fixed when structural deformation occurs. For small elastic deformations, one can write:

$$\mathbf{u}_{G/A} = \mathbf{u}_G - \mathbf{\Psi}_{r,A}\mathbf{u}_{A,b}, \tag{73}$$

$$\mathbf{u}_{A,b} = \begin{bmatrix} \mathbf{I}_3 & -\widetilde{\mathbf{s}_{CA,b}} \\ \mathbf{0}_3 & \mathbf{I}_3 \end{bmatrix} \mathbf{U}_c{}^T \mathbf{u}_G, \tag{74}$$

where $\mathbf{\Psi}_{r,A}$ is the rigid-body mode matrix of the free-free aircraft calculated with origin at A [1] and $\mathbf{U}_C$ is the Boolean matrix that selects the node C degrees of freedom among all DOFs. The left multiplication of Eq. (73) by $\mathbf{K}_{GG}$ and the partition of $\mathbf{u}_{G/A}$ into its fixed DOFs, $\mathbf{u}_{G/A,c} = \mathbf{0}_{6\times 1}$, and free DOFs, $\mathbf{u}_{G/A,f}$, i.e., $\mathbf{u}_{G/A} = \mathbf{U}_f\mathbf{u}_{G/A,f} + \mathbf{U}_c\mathbf{u}_{G/A,c} = \mathbf{U}_f\mathbf{u}_{G/A,f}$, allow one to determine that [1]:

$$\mathbf{u}_{G/A} = \mathbf{U}_f\left(\mathbf{U}_f{}^T\mathbf{K}_{GG}\mathbf{U}_f\right)^{-1}\mathbf{U}_f{}^T\mathbf{K}_{GG}\mathbf{u}_G. \tag{75}$$

The position vector of A in the BRF reads:

$$\mathbf{R}_{A,b} = \mathbf{R}_{O,b} + \mathbf{s}_{OA,b} + \begin{bmatrix} \mathbf{I}_3 & \mathbf{0}_3 \end{bmatrix} \mathbf{u}_{A,b}. \tag{76}$$

A matrix $\mathbf{C}_{ab}$ generated with the small rotations $\boldsymbol{\varphi}_A = \begin{bmatrix} \mathbf{0}_3 & \mathbf{I}_3 \end{bmatrix} \mathbf{u}_{A,b}$:

$$\mathbf{C}_{ab} = \mathbf{I}_3 - \widetilde{\boldsymbol{\varphi}_A} \tag{77}$$

transforms vectors from the BRF to the ARF, such that $\mathbf{R}_A$ is written in the ARF as:

$$\mathbf{R}_{A,a} = \mathbf{C}_{ab}\left(\mathbf{R}_{O,b} + \mathbf{s}_{OA,b} + \begin{bmatrix} \mathbf{I}_3 & \mathbf{0}_3 \end{bmatrix} \mathbf{u}_{A,b}\right). \tag{78}$$

The velocity of A with respect to the wind-tunnel flow, $\mathbf{V}_{w,0} = \begin{Bmatrix} -V_{wt} & 0 & 0 \end{Bmatrix}^T$, then becomes:

$$\begin{aligned} \mathbf{V}_a = {}^0\dot{\mathbf{R}}_{A,a} = \mathbf{C}_{ab}\Big(\mathbf{V}_b + \begin{bmatrix} \mathbf{I}_3 & \mathbf{0}_3 \end{bmatrix} \dot{\mathbf{u}}_{A,b} \\ + \widetilde{\boldsymbol{\omega}_b}\left(\mathbf{s}_{OA,b} + \begin{bmatrix} \mathbf{I}_3 & \mathbf{0}_3 \end{bmatrix} \mathbf{u}_{A,b}\right) + \mathbf{C}_{b0}\begin{Bmatrix} V_{wt} & 0 & 0 \end{Bmatrix}^T\Big). \end{aligned} \tag{79}$$

The acceleration in the ARF with respect to the wind-tunnel flow, assumed of constant speed, is:

$$
\begin{aligned}
{}^{a}\dot{\mathbf{V}}_a = -\widetilde{\boldsymbol{\dot{\varphi}}}_A \Big(\mathbf{V}_b + \begin{bmatrix} \mathbf{I}_3 & \mathbf{0}_3 \end{bmatrix} \dot{\mathbf{u}}_{A,b} + \widetilde{\boldsymbol{\omega}}_b \left(\mathbf{s}_{OA,b} + \begin{bmatrix} \mathbf{I}_3 & \mathbf{0}_3 \end{bmatrix} \mathbf{u}_{A,b} \right) + \mathbf{C}_{b0} \begin{Bmatrix} V_{wt} & 0 & 0 \end{Bmatrix}^T \Big) \\
+ \mathbf{C}_{ab} \Big({}^{b}\dot{\mathbf{V}}_b + \begin{bmatrix} \mathbf{I}_3 & \mathbf{0}_3 \end{bmatrix} \ddot{\mathbf{u}}_{A,b} + {}^{b}\widetilde{\dot{\boldsymbol{\omega}}}_b \left(\mathbf{s}_{OA,b} + \begin{bmatrix} \mathbf{I}_3 & \mathbf{0}_3 \end{bmatrix} \mathbf{u}_{A,b} \right) \\
+ \widetilde{\boldsymbol{\omega}}_b \left(\begin{bmatrix} \mathbf{I}_3 & \mathbf{0}_3 \end{bmatrix} \dot{\mathbf{u}}_{A,b} \right) - \widetilde{\boldsymbol{\omega}}_b \mathbf{C}_{b0} \begin{Bmatrix} V_{wt} & 0 & 0 \end{Bmatrix}^T \Big),
\end{aligned} \tag{80}
$$

from which one obtains the effective aerodynamic velocity and acceleration components:

$$u_a = \mathbf{e}_{3,1}{}^{T0}\dot{\mathbf{R}}_{A,a}, \tag{81}$$
$$v_a = \mathbf{e}_{3,2}{}^{T0}\dot{\mathbf{R}}_{A,a}, \tag{82}$$
$$w_a = \mathbf{e}_{3,3}{}^{T0}\dot{\mathbf{R}}_{A,a}, \tag{83}$$
$$\dot{u}_a = \mathbf{e}_{3,1}{}^{Ta}\dot{\mathbf{V}}_a, \tag{84}$$
$$\dot{v}_a = \mathbf{e}_{3,2}{}^{Ta}\dot{\mathbf{V}}_a, \tag{85}$$
$$\dot{w}_a = \mathbf{e}_{3,3}{}^{Ta}\dot{\mathbf{V}}_a. \tag{86}$$

Knowing u_a, v_a, w_a, $\dot{u}_a$, $\dot{v}_a$, and $\dot{w}_a$, one can calculate the corresponding V_a, α_a, β_a, $\dot{V}_a$, $\dot{\alpha}_a$, and $\dot{\beta}_a$ using the well-known relations, as in Ref. [29]. The inertial angular velocity of the ARF and its derivative in the ARF can be calculated as [1]:

$$\boldsymbol{\omega}_a = \mathbf{C}_{ab}\,\boldsymbol{\omega}_b + \dot{\boldsymbol{\varphi}}_A, \tag{87}$$
$${}^{a}\dot{\boldsymbol{\omega}}_a = -\widetilde{\dot{\boldsymbol{\varphi}}}_A \boldsymbol{\omega}_b + \mathbf{C}_{ab}\,{}^{b}\dot{\boldsymbol{\omega}}_b + \ddot{\boldsymbol{\varphi}}_A, \tag{88}$$

from which the corresponding angular rates and derivatives can be obtained:

$$p_a = \mathbf{e}_{3,1}{}^{T}\boldsymbol{\omega}_a, \tag{89}$$
$$q_a = \mathbf{e}_{3,2}{}^{T}\boldsymbol{\omega}_a, \tag{90}$$
$$r_a = \mathbf{e}_{3,3}{}^{T}\boldsymbol{\omega}_a, \tag{91}$$
$$\dot{p}_a = \mathbf{e}_{3,1}{}^{Ta}\dot{\boldsymbol{\omega}}_a, \tag{92}$$
$$\dot{q}_a = \mathbf{e}_{3,2}{}^{Ta}\dot{\boldsymbol{\omega}}_a, \tag{93}$$
$$\dot{r}_a = \mathbf{e}_{3,3}{}^{Ta}\dot{\boldsymbol{\omega}}_a. \tag{94}$$

The aerodynamic forces and moments due to the rigid-body motion of the ARF are then given by the equations:

$$\mathbf{F}_{a,b} = \bar{q} S_{ref} \mathbf{C}_{ba} \mathbf{C}_{av} \begin{Bmatrix} -C_D & -C_Y & -C_L \end{Bmatrix}^T,$$
$$\mathbf{M}_{a,O,b} = \bar{q} S_{ref} \mathbf{C}_{ba} \begin{Bmatrix} s_w C_l & c_w C_m & s_w C_n \end{Bmatrix}^T + \widetilde{\mathbf{s}_{OA,b}} \mathbf{F}_{a,b}, \tag{95}$$

with $C_i = C_i\left(\alpha_a, \dot{\alpha}_a, \beta_a, \dot{\beta}_a, M, \mathrm{Re}, \omega_a, \delta_c, \ldots\right)$, $i = D, L, Y, l, m, n$ the aerodynamic force or moment coefficients for the rigid aircraft; S_{ref} the reference wing planform area; s_w the reference wing span; c_w the wing mean aerodynamic chord; and $\mathbf{C}_{av}$ given by:

$$\mathbf{C}_{av} = \begin{bmatrix} \cos\alpha_a \cos\beta_a & -\cos\alpha_a \sin\beta_a & -\sin\alpha_a \\ \sin\beta_a & \cos\beta_a & 0 \\ \sin\alpha_a \cos\beta_a & -\sin\alpha_a \sin\beta_a & \cos\alpha_a \end{bmatrix} \tag{96}$$

The incremental forces and moments in the rigid-body DOFs are given by:

$$\Delta\mathbf{F}_{a,b} = \bar{q} \mathbf{C}_{ba} \mathbf{C}_{av} \sum_{k=1}^{N_P} S_k \begin{Bmatrix} -\mathbf{e}_{N_P,k}{}^T \Delta\mathbf{c}_{\mathbf{d,e}} \\ \mathbf{e}_{3,2}{}^T \mathbf{n}_{k,u,b} \left(\mathbf{e}_{N_P,k}{}^T \Delta\mathbf{C}_{\mathbf{p,e}}\right) \\ \mathbf{e}_{3,3}{}^T \mathbf{n}_{k,u,b} \left(\mathbf{e}_{N_P,k}{}^T \Delta\mathbf{C}_{\mathbf{p,e}}\right) \end{Bmatrix}, \tag{97}$$

$$\Delta\mathbf{M}_{a,O,b} = \Delta\mathbf{M}_{0,1} + \Delta\mathbf{M}_{1,0} + \Delta\mathbf{M}_{1,1} + \Delta\mathbf{M}_{A\to O}, \tag{98}$$

$$\Delta\mathbf{M}_{0,1} = \bar{q} \sum_{k=1}^{N_P} S_k \mathbf{C}_{ba} \left(-\,\mathrm{skew}\left(\mathbf{C}_{av} \begin{Bmatrix} -\mathbf{e}_{N_P,k}{}^T \mathbf{c}_{\mathbf{d,u}} \\ \mathbf{e}_{3,2}{}^T \mathbf{n}_{k,u,b} \mathbf{e}_{N_P,k}{}^T \Delta\mathbf{C}_{\mathbf{p,u}} \\ \mathbf{e}_{3,3}{}^T \mathbf{n}_{k,u,b} \mathbf{e}_{N_P,k}{}^T \Delta\mathbf{C}_{\mathbf{p,u}} \end{Bmatrix} \right) \right.$$
$$\left. \mathbf{n}_{k,u,b} \left(\mathbf{e}_{N_P,k}{}^T \mathbf{C}_{025A} \mathbf{G}_{AG} \mathbf{u}_{G/A}\right) \right), \tag{99}$$

$$\Delta\mathbf{M}_{1,0} + \Delta\mathbf{M}_{1,1} = \bar{q} \sum_{k=1}^{N_P} S_k \mathbf{C}_{ba} \left(-\,\mathrm{skew}\left(\mathbf{C}_{av} \begin{Bmatrix} -\mathbf{e}_{N_P,k}{}^T \Delta\mathbf{c}_{\mathbf{d,e}} \\ \mathbf{e}_{3,2}{}^T \mathbf{n}_{k,u,b} \left(\mathbf{e}_{N_P,k}{}^T \Delta\mathbf{C}_{\mathbf{p,e}}\right) \\ \mathbf{e}_{3,3}{}^T \mathbf{n}_{k,u,b} \left(\mathbf{e}_{N_P,k}{}^T \Delta\mathbf{C}_{\mathbf{p,e}}\right) \end{Bmatrix} \right) \right.$$
$$\left. \left(\mathbf{R}_{025,a} \mathbf{e}_{N_P,k} + \mathbf{n}_{k,u,b} \left(\mathbf{e}_{N_P,k}{}^T \mathbf{C}_{025A} \mathbf{G}_{AG} \mathbf{u}_{G/A}\right)\right) \right), \tag{100}$$

$$\Delta\mathbf{M}_{A\to O} = \mathrm{skew}\left(\begin{bmatrix} \mathbf{I}_3 & \mathbf{0}_3 \end{bmatrix} \mathbf{u}_{A,b}\right) \mathbf{F}_{a,b} + \mathrm{skew}\left(\mathbf{s}_{OA,b} + \begin{bmatrix} \mathbf{I}_3 & \mathbf{0}_3 \end{bmatrix} \mathbf{u}_{A,b}\right) \Delta\mathbf{F}_{a,b}, \tag{101}$$

where $\Delta\mathbf{c}_{\mathbf{d,e}} = \Delta\mathbf{c}_{\mathbf{d,ind,e}}$ is the vector of panel drag coefficient disturbances due to the structural deformation, with $\Delta\mathbf{c}_{\mathbf{d,ind,e}}$ the vector of panel induced drag disturbances; $\mathbf{n}_{k,u,b}$ is the normal vector to each panel in its undeformed position, with components written in the BRF coordinate system; $\Delta\mathbf{C}_{\mathbf{p,e}} = \mathbf{A}'\mathbf{w}_{\mathbf{elas}}$; $\mathbf{C}_{025A} \in \mathbb{R}^{N_P \times N_A}$ is a matrix that transforms the aerodynamic grid points' displacements to the normal displacement of the points at 25% of the mean chord of the panels; $\mathbf{R}_{025,a} \in \mathbb{R}^{3\times N_P}$ is a matrix containing the three-dimensional coordinates, in the ARF coordinate system, of the points at 25% of the mean chord of all the panels; $\mathbf{c}_{\mathbf{d,u}} = \mathbf{c}_{\mathbf{d},\mathbf{0}} + \mathbf{c}_{\mathbf{d,ind,u}}$ is the vector of panel drag coefficients due to the rigid-body states: $\mathbf{c}_{\mathbf{d},\mathbf{0}}$ is the vector of panel zero-lift drag coefficients, approximated as $\mathbf{c}_{\mathbf{d},\mathbf{0}} = \sum_{k=1}^{N_P} \mathbf{e}_{N_P,k} \left(S_{ref} / \sum_{k=1}^{N_P} S_k \right) C_{D,0}$; and $\mathbf{c}_{\mathbf{d,ind,u}}$ is the vector of panel induced drag coefficients due to $\Delta\mathbf{C}_{\mathbf{p,u}}$. The induced drag is calculated based on the methodology of Ref. [38].

3 NUMERICAL MODEL

The X-HALE aircraft [27] in its four-meter-span configuration is the aircraft analyzed in the present paper. The four-meter-span configuration contains four wing sections with span of 1.0 m and chord of 0.2 m each, as well as three pods at the connections between the wing panels. At the pods, the aircraft engines, landing gears, electronics and sensors are installed. Booms are connected to the pods and, at the tip of each boom, a horizontal tail is mounted. The two side tails are all-moving control surfaces that can be used for both longitudinal and lateral-directional control, and are then named as elevons. The central tail has a flipping-up capability, in order to modify the aircraft longitudinal and lateral-directional flying qualities as desired in operation. For ground clearance during take-off, the central tail has approximately 33% less span in its right (bottom) part than in the left (top) part. The wing-tip sections have a dihedral angle of 10°. The wing is built with an incidence of 5°.

The aircraft was modeled in the recently developed small-deformation implementation of the ITA/AeroFlex program. Convergence analysis showed that using 96 beam elements along the wing span was an excellent trade-off between an accurate calculation of the modal frequencies less than 50 Hz and general computing time in the calculation of the equilibrium condition, which is done with all the degrees of freedom of the structural-dynamic model – modes of vibration are introduced afterward for time-marching simulations.

The structural-dynamic model was then adjusted to match the measured inertia properties and relevant modal frequencies, as obtained from a ground-vibration test (GVT) previously performed with the aircraft suspended with bungees. The measured inertia properties for the GVT included the aircraft total mass and the concentrated inertias of engines, servos and ballasts. The adjusted modes include the first two symmetric wing bending modes, the first antisymmetric wing bending, fore-and-aft in-plane wing bending and wing torsion modes, as well as lateral bending modes of the booms. After the GVT, the ballasts used were removed and replaced by the aircraft batteries, sensors, transmitters and receivers, the masses and locations of which were measured and included in the computational model. The central pod was also replaced by a metallic one, with which the wind-tunnel mount is connected.

The wind-tunnel strut effective length from a structural-dynamic viewpoint is 1.75 m. At its tip, the aircraft-to-mount connection mechanism with an additional length of 0.215 m is installed. A GVT of the wind-tunnel mount installed in the wind tunnel was also performed, searching for the lowest frequency of the out-of-plane bending modes. The first out-of-plane bending was determined to be at 12.1 Hz, without the aircraft and connection mechanism installed, implying the need to take the mount flexibility into account in the computational model. The mount, together with the connection mechanism (assumed rigid, but with non-negligible inertias), was modeled in the ITA/Aeroflex program using 35 beam elements, and adjusted using its real dimensions and material properties to match the first modal frequency obtained from GVT.

The complete structural-dynamic model assembled in the ITA/AeroFlex program is presented in Fig. 1. The tails and ailerons are assumed rigid. Scalar spring elements are included to represent the stiffness of the motion of all the control surfaces around the corresponding hinge lines, but such stiffnesses are high enough not to modify the results to be obtained.

The rigid-body aerodynamic model of the aircraft is obtained by combining the XFOIL code [39] and the VLM [31] code embedded in ITA/AeroFlex, in the following fashion: the pressure distributions that are provided come from XFOIL runs at different angles of attack and Reynolds

numbers, using either the wing EMX07 [27] or the elevons/horizontal tail NACA 0012 airfoils as geometry. The normalwashes produced by the VLM for a specific angle of attack (AOA) can then be used to calculate the spanwise induced AOAs through an averaging of each strip boxes' normalwashes by the same strip boxes' pressure coefficient differences. These spanwise induced AOAs are then subtracted from the geometrical AOA to allow the determination of new stripwise effective AOAs and corresponding new pressure distributions at each wing or elevon/horizontal tail strip. When the provided and the calculated stripwise induced AOAs are equal to each other within a specified tolerance, the process has converged and one then has a three-dimensional pressure distribution all over the wing and the elevons/horizontal tail. This process is repeated for each angle of attack of the aircraft and for each Reynolds number, allowing the determination of coupled XFOIL-VLM pressure distributions and longitudinal aerodynamic coefficients.

The process also produces the spanwise pressure and friction drag coefficients for all the horizontal lifting surfaces. The spanwise induced drag coefficients can be calculated using the technique of Klmn, Giesing and Rodden [38]. The drag of vertical aircraft components (pods) is calculated using semi-empirical techniques.

However, the rigid-body aerodynamic coefficients also depend on other variables, like the sideslip angle, the body angular rates and the control surface deflections. The dependencies of the rigid-body aerodynamic coefficients on other variables, like the sideslip angle, the body angular rates and the control surface deflections, are also calculated with the complete VLM model, but are adjusted for each different range of angle of attack and value of Reynolds number. The adjustments are provided by classical left-multiplying weighting matrices [36], whose

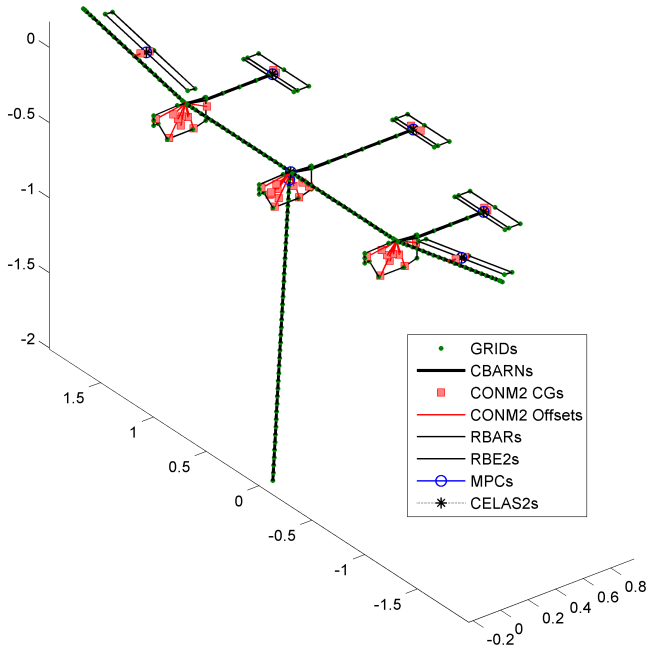

Figure 1: Flexible aircraft and wind-tunnel mount structural-dynamic model with a total of 1530 degrees of freedom, as output from ITA/AeroFlex. Legend entries: GRIDs are the structural nodes; CBARNs are the beam elements; CONM2 CGs are the CG locations of lumped-mass elements; CONM2 Offsets are the offsets between such CG locations and the structural node the lumped-mass element is attached to; RBARs are rigid bar elements; RBE2s are rigid-body elements; MPCs are multi-point constraints; and CELAS2s are scalar spring elements.

diagonal is equal to the nonlinear XFOIL-VLM disturbances in the pressure distribution divided by the linear VLM disturbances due to a given variation in the angle of attack of the aircraft. The pressure distribution of the pods is adjusted with an arbitrary factor of 0.30, due to the absence of the pod fairings in the wind-tunnel test.

The same adjustments are also used in the calculation of the generalized aerodynamic forces in the elastic degrees of freedom. It must be clear that the adjustment is dependent on the ARF angle of attack and Reynolds number, being stored as a look-up table like all the other coefficients.

The VLM mesh used to obtain the rigid-body aerodynamic models is the same one to be used for unsteady aerodynamics calculations in the doublet-lattice method [25]. As such, the VLM model anticipated guidelines that need to be taken into account in the DLM [40]. The resulting VLM/DLM mesh is shown in Fig. 2.

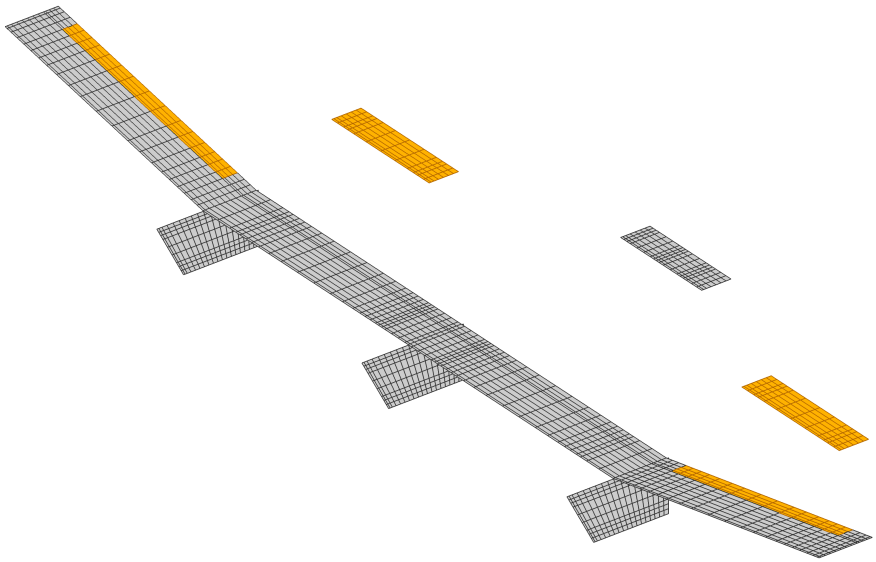

Figure 2: VLM/DLM mesh of the aircraft, with a total of 1908 boxes. Control surfaces are plotted in orange.

In the calculation of the rational function approximations, fifteen different reduced frequencies are used: 0.0001, 0.0010, 0.0123, 0.0489, 0.1090, 0.1910, 0.2929, 0.4122, 0.5460, 0.6910, 0.8436, 1.0000, 1.2500, 1.6000, and 2.0000. A multi-objective optimization using the NSGA-II – Non-Dominated Sorting Genetic Algorithm-II [41] – allowed the determination of an optimum set of lag paremeter values and orders. The chosen RFA is of order 7, with the lag parameter 0.3950 having order 2 and the lag parameter 0.5079 having order 5. An RFA is also generated for the rigid-body degrees of freedom, allowing a representation of the rigid-body unsteady aerodynamics. The rigid-body RFA is also of order 7, with the lag parameter 0.3871 having order 2 and the lag parameter 0.5871 having order 5.

Linear spline interpolation matrices, as derived in Ref. [10], are calculated and used to obtain the displacement-transferal and the load-transferal matrices between the structural-dynamic model and the aerodynamic model.

4 STABILITY OF THE AIRCRAFT WITH CONSTRAINED TRANSLATIONS AND UNCONSTRAINED ROTATIONS

In this section, a numerical study of the effects on dynamic stability of constraining only the aircraft translations in the wind tunnel is done. In order to more closely represent the aircraft flight shape, the trimming algorithm solves for equilibrium with null support reactions at the aircraft-to-mount connection, $\lambda_{13} = \lambda_{14} = \lambda_{15} = 0$. Wind-tunnel speed of 14 m/s is considered. The aircraft is trimmed for a null sideslip angle.

The trimmed condition states, controls and wing tip displacements and twist angles obtained for the free aircraft and for the 3-DOF-constrained aircraft are summarized in Table 1. The small differences have a reason: whereas the 3-DOF-constrained aircraft must have null moments about the connection point with the mount (located approximately 0.011 m forward and 0.046 m downward of the structural node at the wing symmetry plane), the free aircraft must have null total moments about its CG, which is located, in the deformed condition, approximately 0.027 m rearward and 0.019 m downward of the same structural node.

	Free aircraft	3-DOF constrained	Units
Angle of attack (α)	1.222	1.226	deg
Left elevon deflection (δ_{le})	4.884	4.887	deg
Right elevon deflection (δ_{re})	4.794	4.797	deg
Left engine thrust (T_l)	1.085	1.085	N
Central engine thrust (T_c)	1.086	1.086	N
Right engine thrust (T_r)	1.087	1.087	N
Left wing tip vert. displacement ($d_{z,lwt,b}$)	-0.050	-0.050	m
Right wing tip vert. displacement ($d_{z,rwt,b}$)	-0.050	-0.050	m
Left wing tip twist angle ($\theta_{lwt,b}$)	-0.121	-0.126	deg
Right wing tip twist angle ($\theta_{rwt,b}$)	-0.100	-0.105	deg

Table 1: Trimmed condition of the free aircraft in level flight at 14 m/s and of the 3-DOF-constrained aircraft without support reactions at 14 m/s of wind-tunnel speed.

Considering that the trimmed conditions are practically the same, the dynamic stability of the aircraft can then be compared for the two cases based on the linearization of the equations of motion. Stiffness-proportional damping is assumed, such that the first free-free mode of vibration of the aircraft has 1.5% damping ratio, and the first strut constrained mode of vibration has 3.0% damping ratio. Aircraft and strut modes of vibration up to 25 Hz are kept in the equations of motion. The obtained eigenvalues are plotted in Fig. 3.

The phugoid mode naturally disappears in the constrained aircraft. Little modification occurs for the roll subsidence mode, which is expected since the roll damping of the aircraft is not much affected by the constraints. The first aeroelastic mode, dominantly consisting of symmetric wing bending, is also only slightly affected. However, the same cannot be stated with respect to the short-period and Dutch-roll modes. The former loses damping mainly because there is no difference between $\dot{\alpha}_a$ and q_a in a wind-tunnel at constant speed. The latter, however, becomes significantly unstable for this configuration, due to the absence of a vertical tail or vertical fins providing directional stability about the aircraft-to-mount connection. Actually, the pods are potentially destabilizing for this configuration.

The instability of the Dutch-roll mode was faced in practice in the first wind-tunnel test run for the X-HALE at the TA-2 wind tunnel, on March 15, 2017. The aircraft was uncontrollable

even at very low speeds, and the test ended prematurely with the failure of both aluminum L brackets [27] connecting the central modified metallic pod to the wing, due to excessive bending moment.

5 WIND-TUNNEL TEST

Experiments have been run in the TA-2 subsonic wind tunnel at the Institute of Aeronautics and Space (IAE), Brazil. The experimental setup inside the wind tunnel can be seen in Fig. 4. The aircraft is mounted on a strut, on top of a hinge that constrains yawing and pitching angular motions, but leaves the aircraft free to roll up to ± 12 degrees. For safety reasons, lateral cables connecting the external booms to the ground limit the rolling motion to ± 10 degrees.

The aircraft is equipped with a Microbotics MIDG II INS/GPS system at the central pod combining a three-axis accelerometer, GPS, and gyroscope into a small self-contained unit. This single unit acts as an inertial navigation system that will in the future provide the aircraft controller data regarding the position and orientation of the aircraft. The angular rate sensor's accuracy of $0.05^\circ/\text{sec}$ and linear acceleration sensor accuracy of 150 μg provide the necessary accuracy for code validation. Two Pitot tubes at the wing tips, another Pitot tube in the inner right section of the wing, and an additional Pitot tube on the ground of the wind tunnel provide information on the wind speed.

A camera is positioned behind the aircraft and the recorded video is displayed in real-time on a screen outside the wind tunnel available to the test pilot, as shown in Fig. 5. A lateral GoPro camera fixed to the wind-tunnel wall and focusing the left wing tip helps to observe the elevons' deflections and their effect on wing torsion. Due to the large wing span compared with the wind-tunnel sections, the aircraft is positioned downstream of the test section and is therefore subjected to non-modeled flow turbulence. Despite this effect, overall rolling motions were well captured by the MIDG unit.

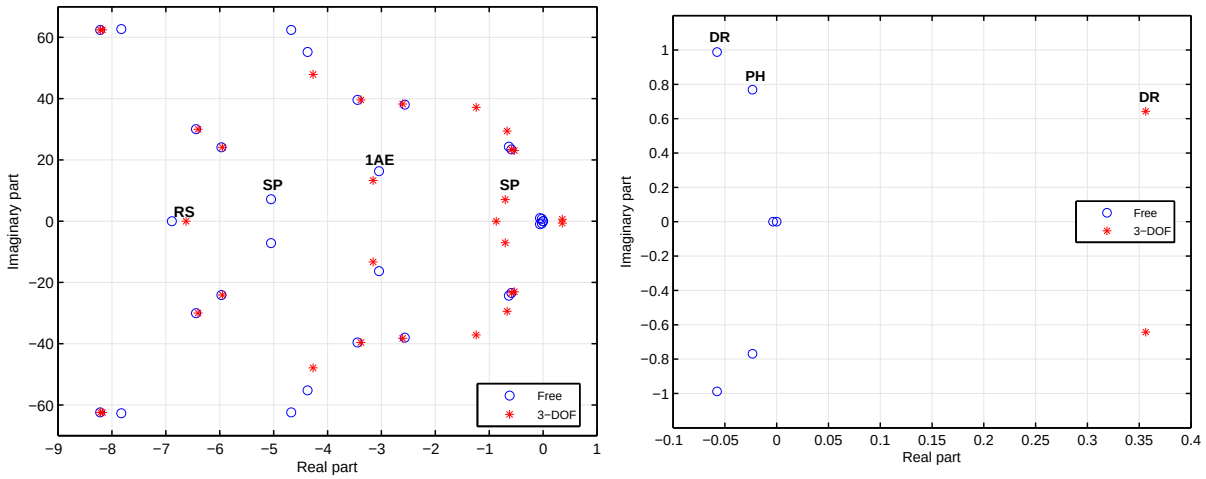

Figure 3: Eigenvalues of the linearized dynamics of the free aircraft in level flight at 14 m/s and of the 3-DOF-constrained aircraft without support reactions at 14 m/s of wind-tunnel speed. Short-period (SP), first aeroelastic (1AE), roll subsidence (RS), Dutch-roll (DR), and phugoid (PH) modes' eigenvalues are highlighted.

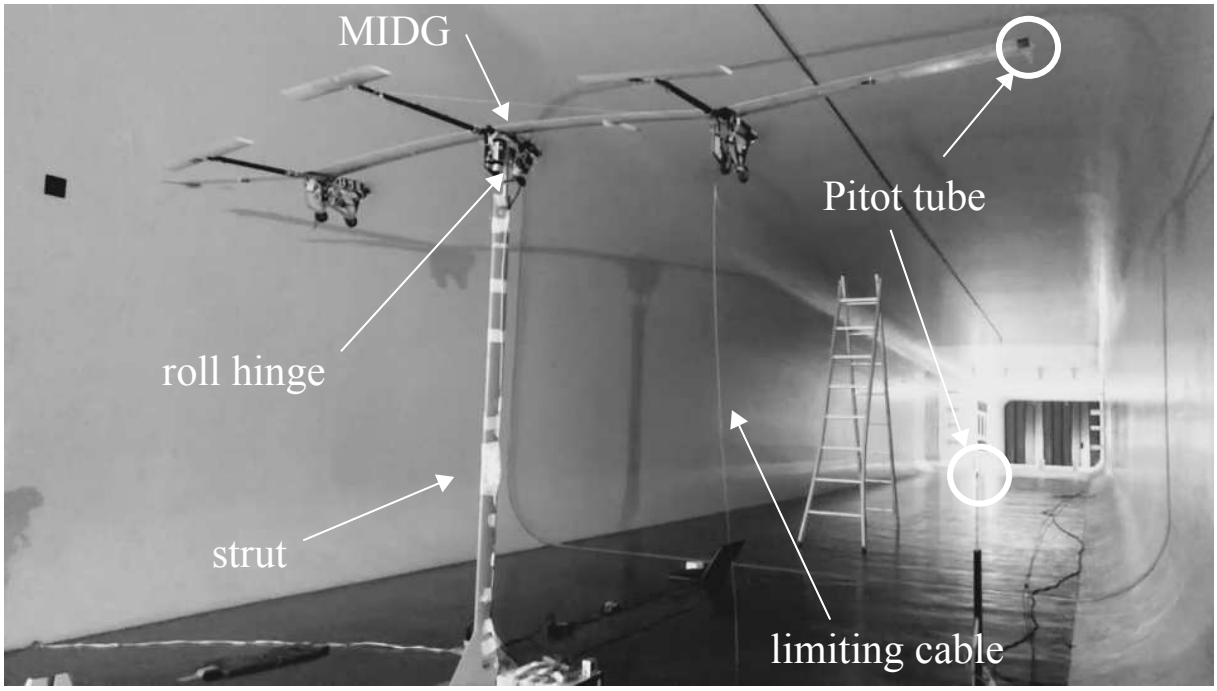

Figure 4: X-HALE in the TA-2 wind tunnel, mounted on a strut with a roll hinge at the connection.

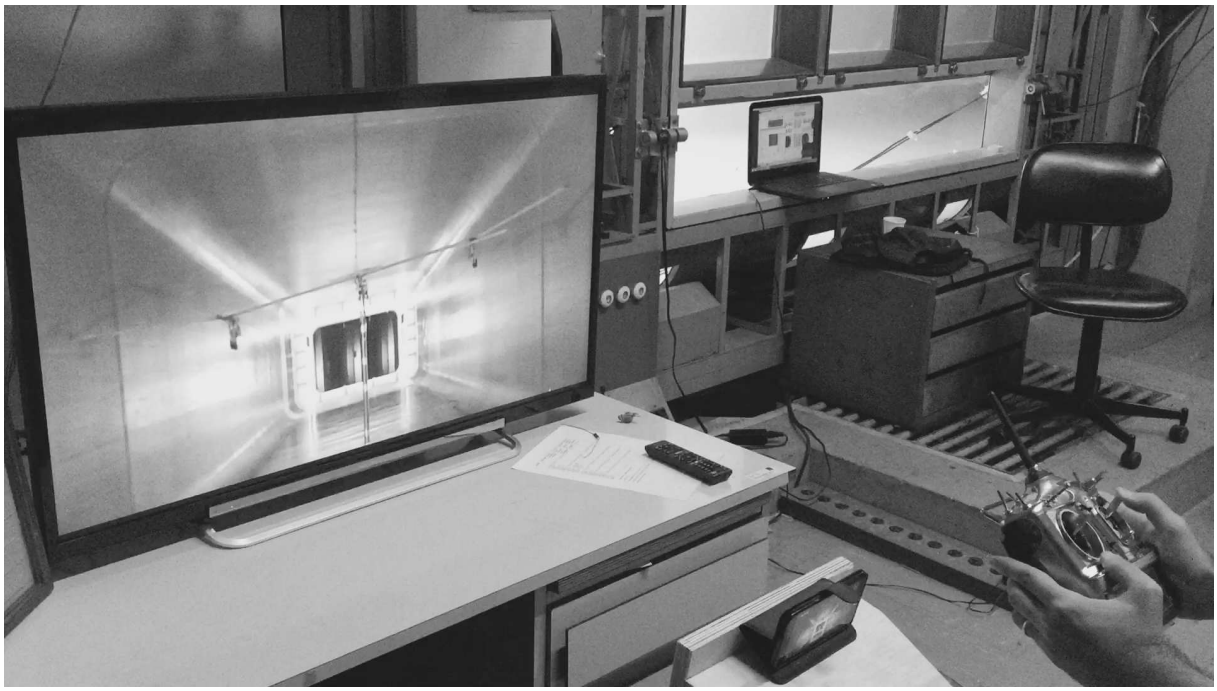

Figure 5: Execution of the wind tunnel test by the test pilot.

6 CORRELATION BETWEEN EXPERIMENTAL AND NUMERICAL RESULTS

The results to be presented and analyzed in this section refer to the aircraft with only the roll DOF left free.

Computational simulations were run for the aircraft subjected both to anti-symmetrical elevon doublets and to anti-symmetrical aileron doublets. The referred control surfaces can be seen in Figs. 1 and 2. Time histories are presented in Figs. 6 and 7 for the aileron command and 8 and 9 for the elevon command.

Figures 6 and 7 show that nothing unusual is predicted by the numerical model with respect to aileron deflections in normal operating flight speeds. As the wind tunnel speed increases, aileron roll control effectiveness increases. It can be seen that the elastic twist angles induced by aileron deflection are relatively small at the wing tip. The induced bending is also on the order of centimeters.

However, the same cannot be said for the elevons. Figures 8 and 9 show a clear reversal in elevon roll control between 8 m/s and 10 m/s (closer to the latter). Aircraft roll response to aileron commands are also much sluggish at speeds below 8 m/s. Since the aircraft will hardly operate below 10 m/s, it can be considered that the elevons are in reversal in the whole flight envelope of the X-HALE aircraft.

The numerical results indicate that the ailerons are more effective in roll control than the elevons, due to the faster responses.

Positive elevon deflections induce considerable negative elastic twist angle disturbances at the semi-wing lying on the same side as the deflected elevon, and vice-versa. Wing bending, on the other hand, is not significantly affected. The reversal mechanism was clearly observed in the wind-tunnel tests, as illustrated by the video frames shown in Fig. 10.

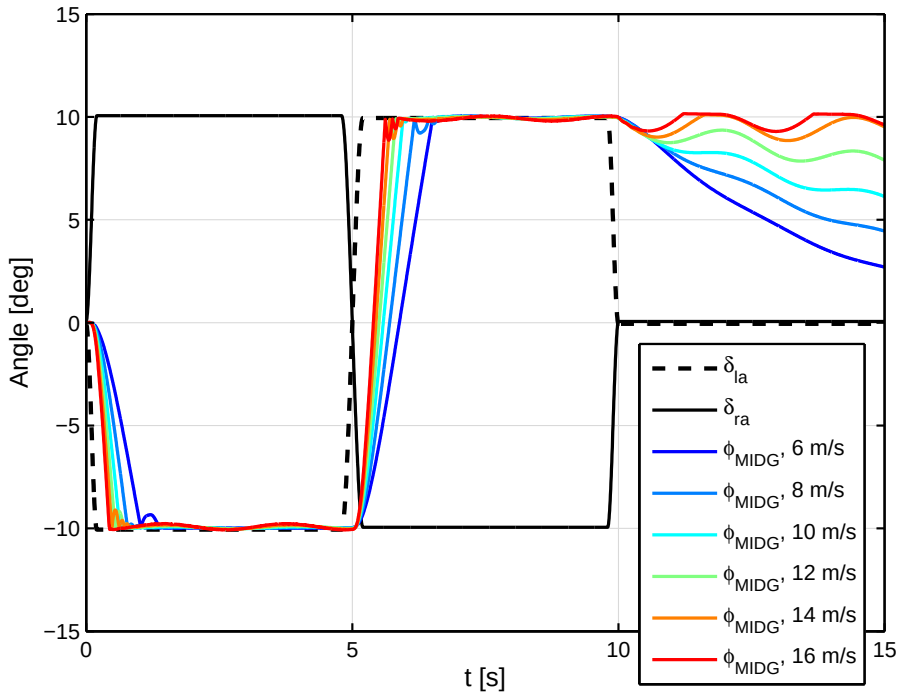

Figure 6: Anti-symmetrical aileron doublet and the roll angle as it would be measured by the MIDG system, at different wind tunnel speeds.

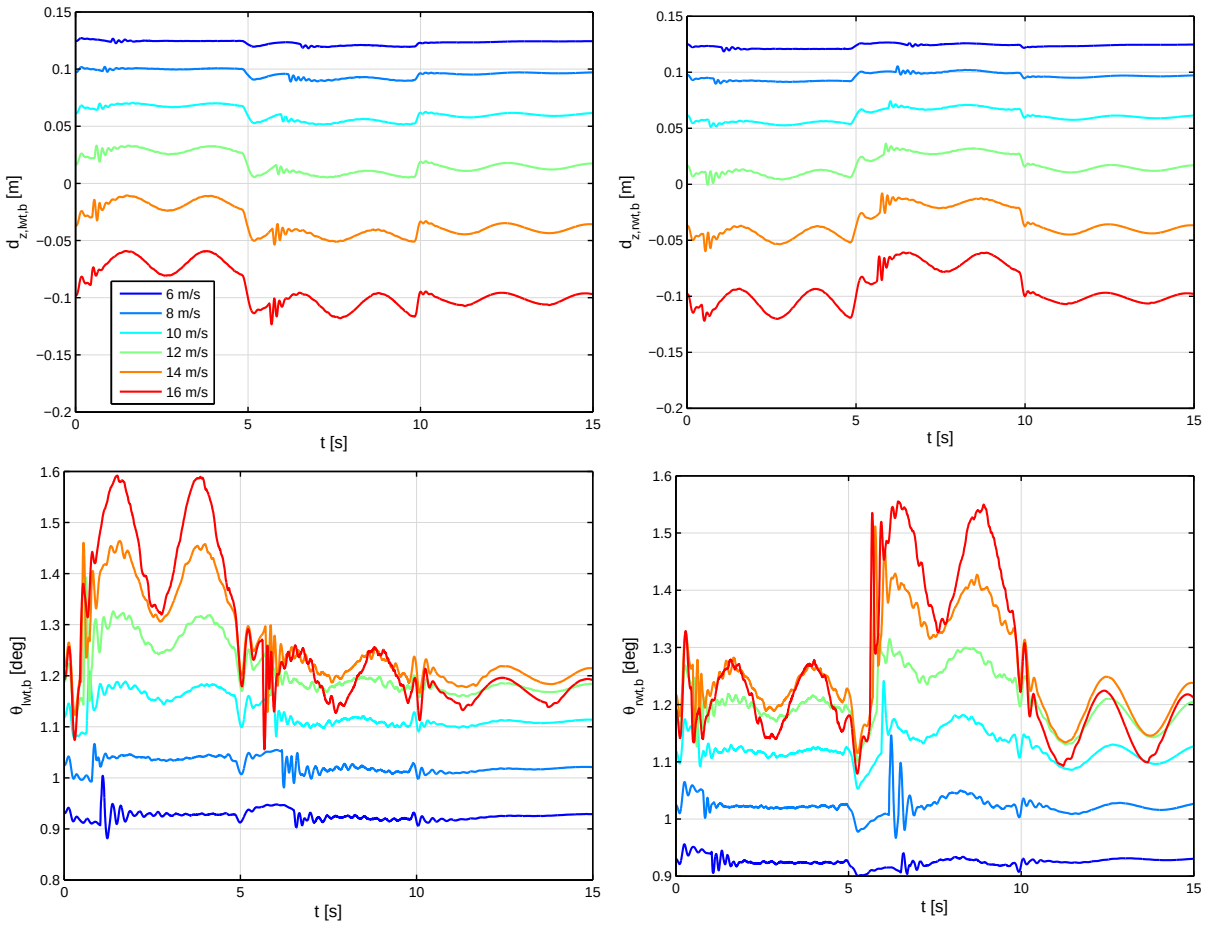

Figure 7: Left and right wing tip vertical displacements (positive down) and twist angles due to the anti-symmetrical aileron doublet.

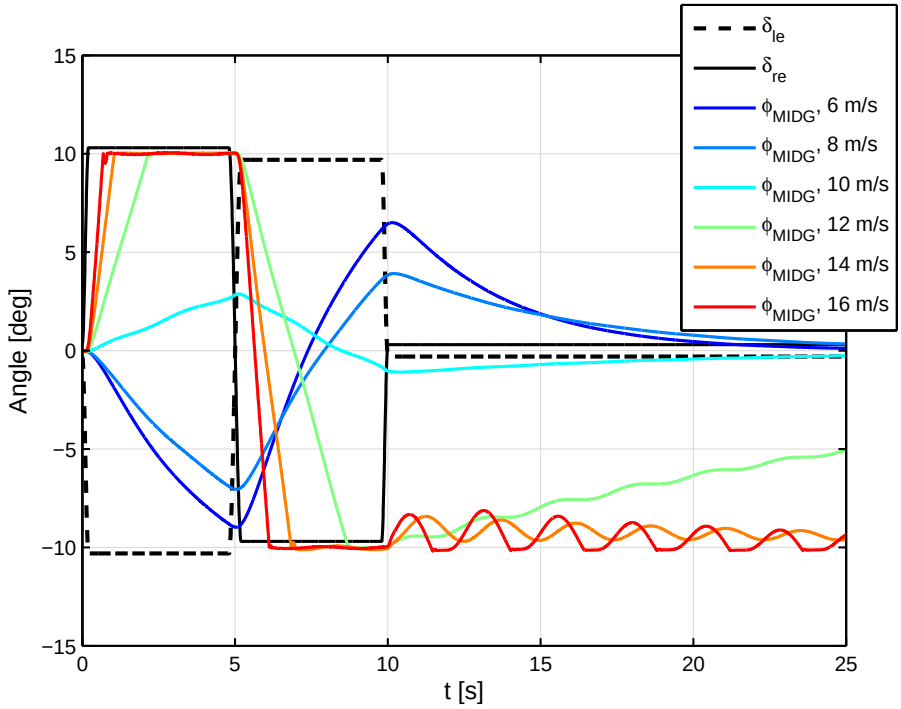

Figure 8: Anti-symmetrical elevon doublet and the roll angle as it would be measured by the MIDG system, at different wind tunnel speeds.

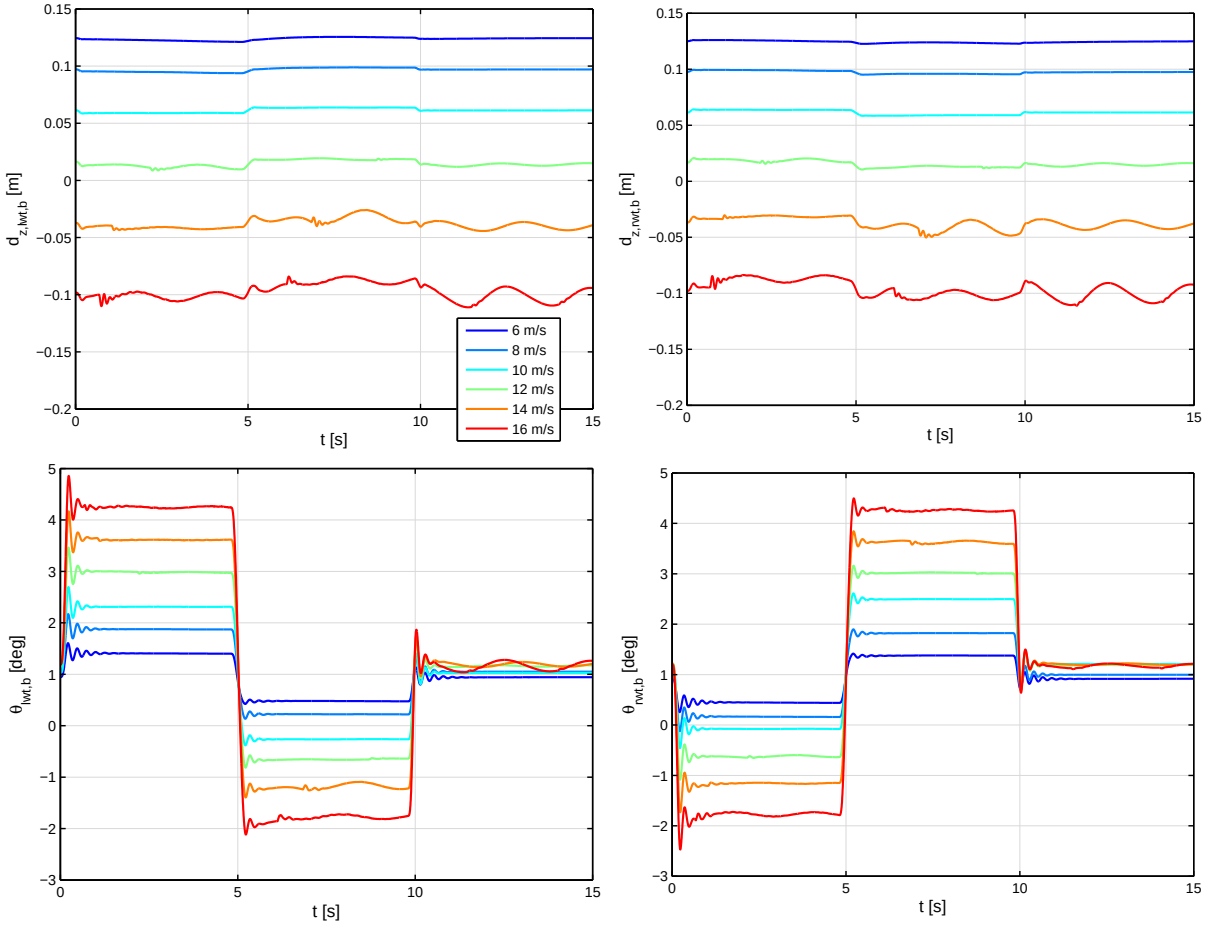

Figure 9: Left and right wing tip vertical displacements (positive down) and twist angles due to the anti-symmetrical elevon doublet.

Time histories were also recorded during the wind-tunnel tests, and selected time intervals of the response of the bank angle measured by the MIDG are shown in Figs. 11 and 12, for the aileron roll control test and for the elevon roll control test, respectively. In such time intervals, the engines were off, but the propellers were windmilling, an effect that is by no means considered in the numerical model. The actual control surface deflections were not measured. Instead, the pulse width modulation (PWM) commands were recorded. Their conversion to commanded deflections were determined prior to the beginning of each test, by physically measuring the control surface deflection angle while a PWM command was being received and recorded. At last, the MIDG measured bank angle is considered to have an uncertainty of $\pm$ 1.0 deg, based on the system data sheets.

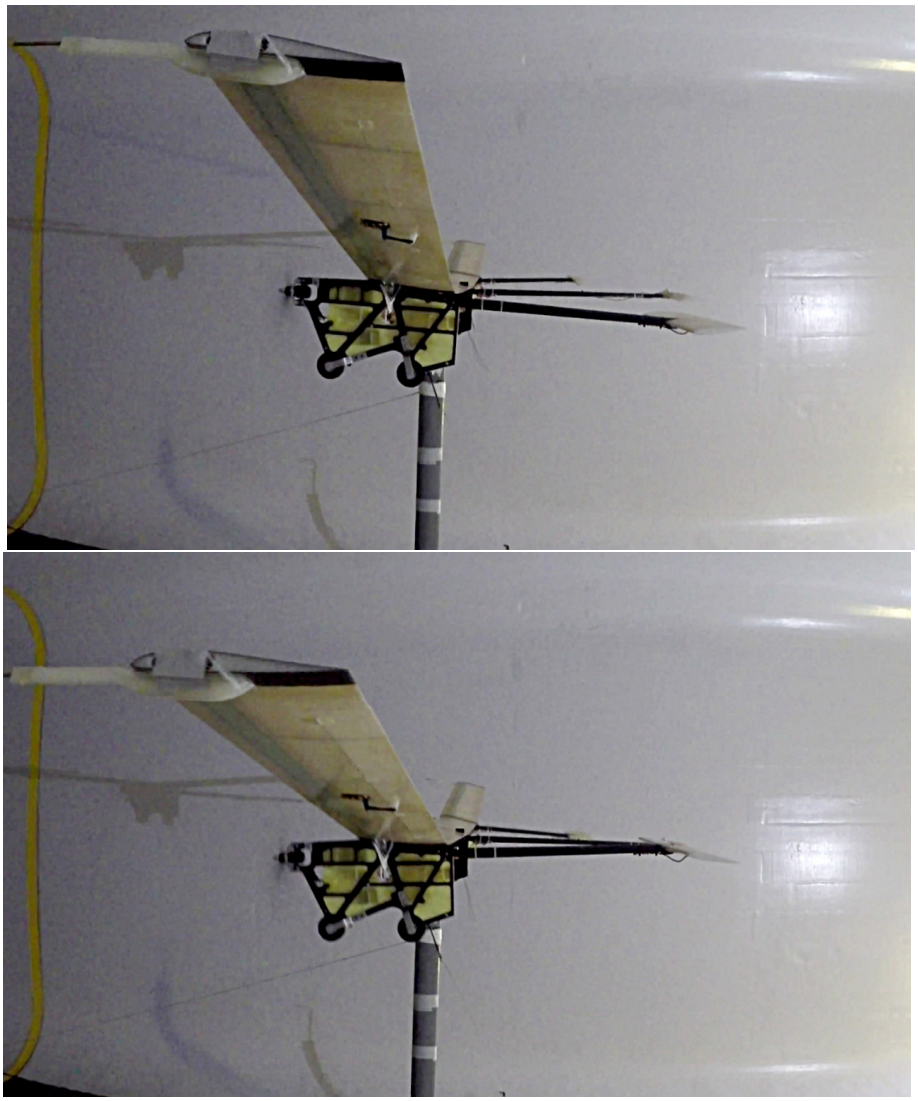

Figure 10: The mechanism of elevon roll control reversal in two different frames of the video captured during the wind-tunnel elevon roll control test. In the top frame, negative left elevon deflection induces positive wing twist. In the bottom frame, positive left elevon induces negative wing twist. The central boom is near the roll hinge line and served as reference for these observations.

In the experimental results, no reversal is observed for the aileron roll control, but the reversal is seen to occur between 8 m/s and 11 m/s. The test pilot opinion was that the aircraft was much less responsive between such speeds.

More extensive quantitative comparison between the wind-tunnel and the numerical results is unfortunately precluded by some facts that the reader should be aware of. The aircraft had to be installed downstream of the test section, due to the wing span, and was then subjected to stronger turbulence effects. After the test using elevons to roll the aircraft, it was found that the left elevon presented nonlinearity in its deflection response to a pilot command, which may explain the asymmetry of the bank angle measured by the MIDG about 0 deg in Fig. 12. Nonlinearities due to the limiting cables were also not included in the numerical model. At last, the metallic pod used to allow the connection of the aircraft to the wind-tunnel mount did not have its flexibility taken into account in the numerical model.

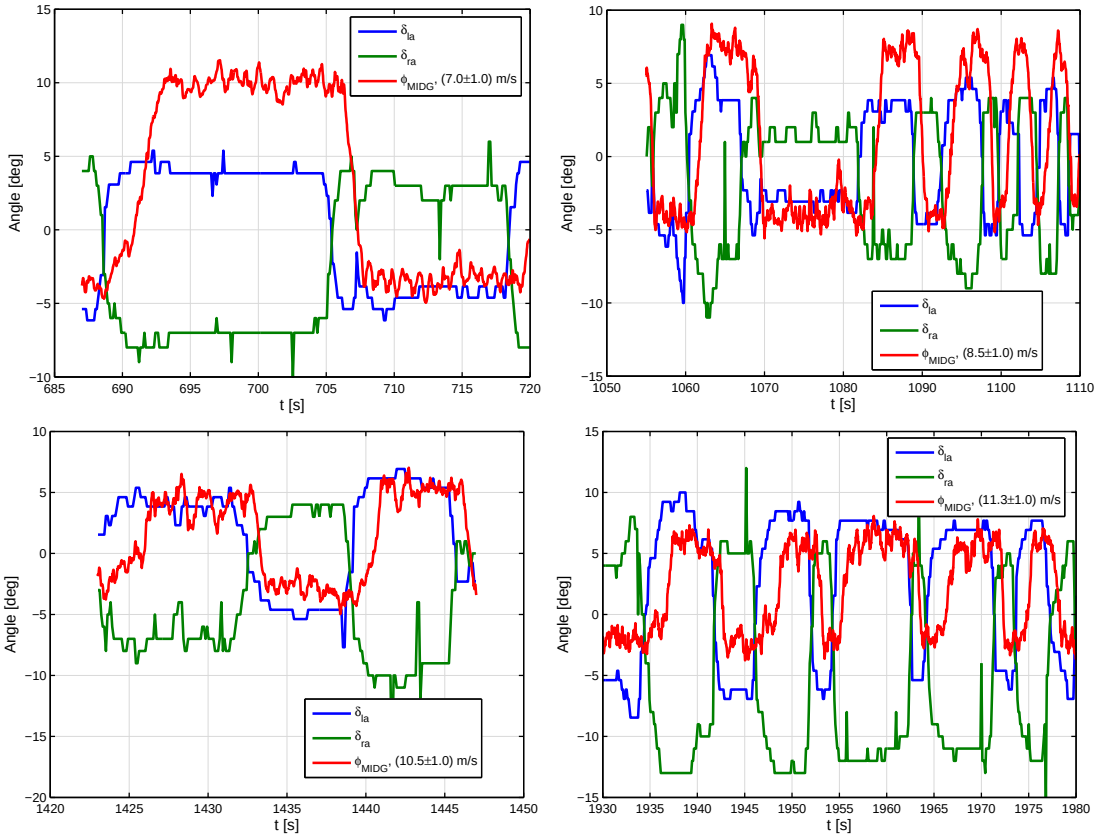

Figure 11: Recorded anti-symmetrical aileron commands and roll angle measured by the MIDG system, at different wind tunnel speeds.

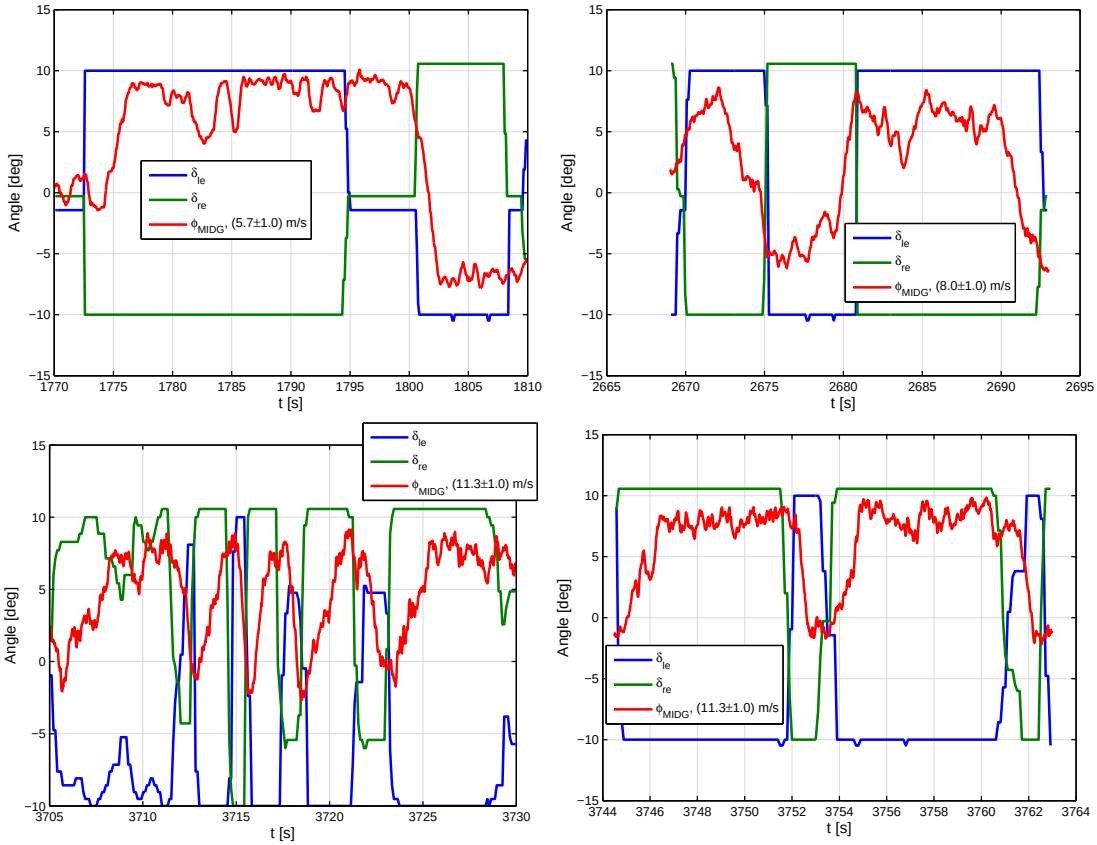

Figure 12: Recorded anti-symmetrical elevon commands and roll angle measured by the MIDG system, at different wind tunnel speeds.

7 CONCLUDING REMARKS

A formulation for the dynamics of constrained aircraft in wind tunnel was derived and implemented, aimed at allowing the determination of response and stability characteristics. Holonomic constraints were included in Lagrange's equations to allow the inclusion of up to three rotational constraints to the aircraft rigid-body motion. In the formulation, the aircraft rigid-body translations are all constrained, but vary in time due to the consideration that the wind-tunnel mount to which the aircraft is connected is flexible.

The effect of constraining only the translations was illustrated with the comparison of the dynamic modes of the X-HALE aircraft in free flight and in wind tunnel with the three translational degrees of freedom constrained. An unstable Dutch-roll mode was obtained for the constrained aircraft, and significant loss of the short-period damping was also observed. No flutter mode developed.

The four-meter-span configuration of the remotely-piloted X-HALE was tested in the IAE TA-2 wind tunnel in Brazil. A computational model of the tested aircraft was built and the formulation proposed in this paper was used to determine the aircraft response characteristics to anti-symmetric aileron or elevon deflections. Elevon roll control reversal was obtained both numerically and experimentally, and the velocity range in which the phenomenon occurs is in good agreement between both results, around 9 m/s. Aileron roll control is not reverted in normal operation.

The good correlation between numerical and experimental results indicate that the wind-tunnel test campaign was successful and also that the implemented formulations and created numerical models are preliminarily approved for the next steps of validation, which will include flight tests.

8 REFERENCES

[1] Guimarães Neto, A. B., Silva, R. G. A., Paglione, P., and Silvestre, F. J., "Formulation of the flight dynamics of flexible aircraft using general body axes," *AIAA Journal*, Vol. 54, No. 11, 2016, pp. 3516–3534. DOI: 10.2514/1.J054752.

[2] Bisplinghoff, R. L., Ashley, H., and Halfman, R. L., *Aeroelasticity*, Addison-Wesley Publishing Company, Inc., 1955.

[3] Bisplinghoff, R. L., and Ashley, H., *Principles of aeroelasticity*, Dover Publications, Inc., 1962.

[4] Etkin, B., *Dynamics of Flight Stability and Control*, John Wiley & Sons, Inc., 1959.

[5] Dusto, A. R., Brune, G. W., Dornfeld, G. M., Mercer, J. E., Pilet, S. C., Rubbert, P. E., Schwanz, R. C., Smutny, P., Tinoco, E. N., and Weber, J. A., "A method for predicting the stability characteristics of an elastic airplane: FLEXSTAB theoretical description," NASA-CR-114712., 1974 *apud* Abzug, M. J., and Larrabee, E. E., *Airplane stability and control:* a history of the technologies that made aviation possible, 2nd ed. Cambridge: University Press, 2002.

[6] Perkin, B. R., and Erickson, L. L., "FLEXSTAB - A Computer Program for the Prediction of Loads and Stability and Control of Flexible Aircraft," *Proceedings of the SCAR Conference*, Part 1, NASA CP-001, November, 1976.

[7] Milne, R. D., "Dynamics of the Derformable Aeroplane," Technical Report R&M 3345, Her Majestys Stationary Office, London, England, 1964.

[8] Lamb, H., *Higher Mechanics*, 2nd ed. Cambridge: University Press, 1929.

[9] Rodden, W. P., and Love, J. R., "Equations of Motion of a Quasisteady Flight Vehicle Utilizing Restrained Static Aeroelastic Characteristics," *Journal of Aircraft*, Vol. 22, No. 9, 1985, pp. 802-809.

[10] Rodden, W. P., and Johnson, E. H., *MSC.NASTRAN Aeroelastic Analysis User's Guide*, MacNeal-Schwendler Corporation, Los Angeles, 1994, Chap. 2.

[11] Dykman, J. R., and Rodden, W. P., "Structural Dynamics and Quasistatic Aeroelastic Equations of Motion," *Journal of Aircraft*, Vol. 37, No. 3, 2000, pp. 538–542.

[12] Waszak, M. R., and Schmidt, D. K., "Flight Dynamics of Aeroelastic Vehicles," *Journal of Aircraft*, Vol. 25, No. 6, 1988, pp. 563-571.

[13] Cavin III, R. K., and Dusto, A. R., "Hamilton's Principle: Finite-Element Methods and Flexible Body Dynamics," *AIAA Journal*, Vol. 15, No. 12, 1977, pp. 1684-1690.

[14] Buttrill, C. S., Zeiler, T. A., and Arbuckle, P. D., "Nonlinear Simulation of a Flexible Aircraft in Maneuvering Flight," *AIAA Flight Simulation Technologies Conference*, AIAA 87-2501, Monterey, California, Aug. 17-19, 1987.

[15] Zeiler, T. A., and Buttrill, C. S., "Dynamic Analysis of an Unrestrained, Rotating Structure through Nonlinear Simulation," *Structures, Structural Dynamics and Materials Conference*, AIAA-1988-2232, Apr. 18-20, 1988.

[16] Meirovitch, L., and Tuzcu, I., "Unified Theory for the Dynamics and Control of Maneuvering Flexible Aircraft," *AIAA Journal*, Vol. 42, No. 4, 2004, pp. 714-727.

[17] Meirovitch, L., *Methods of analytical dynamics*, Dover, Inc., 2003.

[18] Meirovitch, L., and Tuzcu, I., "Time simulations of the Response of Maneuvering Flexible Aircraft," *Journal of Guidance, Control and Dynamics*, Vol. 27, No. 5, 2004, pp. 814–828.

[19] Reschke, C., "Flight Loads Analysis with Inertially Coupled Equations of Motion," *AIAA Atmospheric Flight Mechanics Conference and Exhibit*, AIAA 2005-6026, San Francisco, California, Aug. 15-18, 2005.

[20] Reschke, C., *Integrated Flight Loads Modelling and Analysis for Flexible Transport Aircraft*, Dissertation for a Doctoral Degree, Institut Flugmechanik und Flugregelung der Universitat Stuttgart, 2006.

[21] Baldelli, D. H., Chen, P. C., and Panza, J., "Unified aeroelastic and flight dynamic formulation via rational function approximations," *Journal of Aircraft*, Vol. 43, No. 3, 2006, pp. 763–772.

[22] Guimarães Neto, A. B., *Flight dynamics of flexible aircraft using general body axes: a theoretical and computational study*, Thesis (PhD in Aeronautical and Mechanical Engineering) – Instituto Tecnológico de Aeronáutica, São José dos Campos, Brazil, 2014.

[23] Hesse, H., and Palacios, R., "Consistent structural linearisation in flexible-body dynamics with large rigid-body motion," *Computers & Structures*, Vol. 110-111, Nov. 2012, pp. 1–14. DOI: 10.1016/j.compstruc.2012.05.011.

[24] Eversman, W., and Tewari, A., "Consistent rational function approximation for unsteady aerodynamics," *Journal of Aircraft*, Vol. 29, No. 9, 1991, pp. 545–552.

[25] Albano, E., and Rodden, W. P., "A doublet-lattice method for calculating lift distributions on oscillating surfaces in subsonic flows," *AIAA Journal*, Vol. 7, No. 2, 1969, pp. 279–285, DOI: 10.2514/3.5086.

[26] Farmer, M. G., "A two-degree-of-freedom flutter mount system with low damping for testing rigid wings at different angles of attack," NASA-TM-83302, 1982.

[27] Cesnik, C. E. S., Senatore, P. J., Su, W., Atkins, E. M., and Shearer, C. M., "X-HALE: A Very Flexible Unmanned Aerial Vehicle for Nonlinear Aeroelastic Tests," *AIAA Journal*, Vol. 50, No. 12, 2012, pp. 2820–2833.

[28] Flannery, M. R., "The enigma of nonholonomic constraints," *American Journal of Physics*, Vol. 73, No. 3, 2005, pp. 265–272. DOI: 10.1119/1.1830501.

[29] Stevens, B. L., and Lewis, F. L., *Aircraft control and simulation*, Wiley, Hoboken, NJ, 2003, pp. 25–29; 116–138; 263–265.

[30] Bismarck-Nasr, M. N., *Structural Dynamics in Aeronautical Engineering*, AIAA Education Series, AIAA, Reston, VA, 1999, pp. 53–91.

[31] Hedman, S. G., "Vortex Lattice Method for Calculation of Quasi Steady State Loadings on Thin Elastic Wings," Aeronautical Research Inst. of Sweden Rept. 105, Stockholm, 1965.

[32] Craig Jr., R. R., and Kurdila, A. J., *Fundamentals of structural dynamics*, Wiley, Hoboken, NJ, 2006, pp. 539–544.

[33] Przemieniecki, J. S., *Theory of Matrix Structural Analysis*, McGrawHill, New York, 1968, pp. 129-148.

[34] Giesing, J. P., Klmn, T. P., and Rodden, W. P., *Correction factor techniques for improving aerodynamic prediction methods*, NASA-CR-144967, 1976.

[35] Silva, R. G. A., Mello, O. A. F., Azevedo, J. L. F., Chen, P. C., and Liu, D. D., "Investigation on transonic correction methods for unsteady aerodynamics and aeroelastic analyses," *Journal of Aircraft*, Vol. 45, No. 6, 2008, pp. 1890–1903. DOI: 10.2514/1.33406.

[36] Guimarães Neto, A. B., Silva, R. G. A., and Paglione, P., "Control-point-placement method for the aerodynamic correction of the vortex-and the doublet-lattice methods," *Aerospace Science and Technology*, Vol. 37, 2014, pp. 117–129. DOI: 10.1016/j.ast.2014.05.007.

[37] Roger, K. L., *Airplane math modeling methods for active control design*, AGARD-CP-228, 1977.

[38] Kálmán, T. P., Giesing, J. P., and Rodden, W. P, "Spanwise distribution of induced drag in subsonic flow by the vortex lattice method," *Journal of Aircraft*, Vol. 7, No. 6, 1970, pp. 574–576.

[39] Drela, M., "XFOIL: An analysis and design system for low Reynolds number airfoils," In: T. Mueller, editor, *Low Reynolds Number Aerodynamics*, Vol. 54 of Lecture Notes in Engineering, pp. 1–12. Springer Berlin Heidelberg, 1989.

[40] Rodden, W. P., Taylor, P. F., McIntosh, S. C., and Baker, M. L., "Further Convergence Studies of the Enhanced Doublet-Lattice Method," *Journal of Aircraft*, Vol. 36, No. 4, 1999, pp. 682–688. DOI: 10.2514/2.2511.

[41] Deb, K., et al., "A fast and elitist multiobjective genetic algorithm: NSGA-II," *IEEE Transactions on Evolutionary Computation*, Vol. 6, No. 2, 2002, pp. 182–197.

COPYRIGHT STATEMENT